

DOT/FAA/AR-97/53

Office of Aviation Research
Washington, D.C. 20591

Advanced Armor Technology: Application Potential for Engine Fragment Barriers for Commercial Aircraft

September 1997

Final Report

This document is available to the U.S. public
through the National Technical Information
Service, Springfield, Virginia 22161.



U.S. Department of Transportation
Federal Aviation Administration

NOTICE

This document is disseminated under the sponsorship of the U.S. Department of Transportation in the interest of information exchange. The United States Government assumes no liability for the contents or use thereof. The United States Government does not endorse products or manufacturers. Trade or manufacturer's names appear herein solely because they are considered essential to the objective of this report.

This report is available at the Federal Aviation Administration William J. Hughes Technical Center's Full-Text Technical Reports page: www.tc.faa.gov/its/act141/reportpage.html in Adobe Acrobat portable document format (PDF).

1. Report No. DOT/FAA/AR-97/53		2. Government Accession No.		3. Recipient's Catalog No.	
4. Title and Subtitle ADVANCED ARMOR TECHNOLOGY: APPLICATION POTENTIAL FOR ENGINE FRAGMENT BARRIERS FOR COMMERCIAL AIRCRAFT				5. Report Date September 1997	
				6. Performing Organization Code	
7. Author(s) D. A. Shockey, J. H. Giovanola, J. W. Simons, D.C. Erlich, R.W. Klopp, and S.R. Skaggs				8. Performing Organization Report No. PYU-7412	
9. Performing Organization Name and Address SRI International 33 Ravenswood Avenue Menlo Park, CA 94025-3493				10. Work Unit No. (TRAIS)	
				11. Contract or Grant No. 95-G-010	
12. Sponsoring Agency Name and Address U.S. Department of Transportation Federal Aviation Administration William J. Hughes Technical Center Atlantic City International Airport, NJ 08405				13. Type of Report and Period Covered Final Report	
				14. Sponsoring Agency Code AAR-431	
15. Supplementary Notes FAA William J. Hughes Technical Center COTR: William Emmerling					
16. Abstract On rare occasions, aircraft turbine engines fail catastrophically and send into the aircraft fragments that disrupt control, fuel, and propulsion systems and jeopardized the ability of the aircraft to land safely. To enhance the survivability of commercial aircraft in the event of an uncontained turbine engine failure, the Federal Aviation Administration (FAA) is sponsoring a research program aimed at protecting components of the aircraft that are critical to continued safe flight and landing. As a member of the FAA contractor team, SRI International is attempting to identify technology transfer opportunities for aircraft engine fragment barriers by surveying the recent advances in Department of Defense (DoD) armor structures. This report review the current state of military armor technology and identifies concepts, materials, and designs that may be useful in developing engine fragment barriers with low added weight and cost. Based on the findings, fragment barrier designs are postulated. Their feasibility has begun to be evaluated by performing fragment impact calculations and experiments. This work has confirmed high-strength polymer fibers as the advanced material most appropriate for protecting aircraft from engine fragments and has identified three particular polymers (fibers of aramids, polyethylenes, and polybenzoxazole) as having the prerequisite of low density and high strength. Furthermore, these materials appear to have sufficient flame resistance, water absorption resistance, and thermal and acoustic insulation properties to serve as building blocks for barriers. The next step is to design practical barriers from these fibers.					
17. Key Words Armor technology transfer, Fragment barriers, Uncontainment, Advanced armor materials, High strength polymer fibers, PBO			18. Distribution Statement This document is available to the public through the National Technical Information Service, Springfield, Virginia 22161		
19. Security Classif. (of this report) Unclassified		20. Security Classif. (of this page) Unclassified		21. No. of Pages 76	22. Price N/A

ACKNOWLEDGMENTS

We were assisted by many people in performing this work. We are grateful to Bob Pursel, Bill Emmerling, Mike Dostert, and Tim Mousakis of the FAA and Phil Sallee and Javaid Nazir of Boeing Commercial Airplane Group for their encouragement and interest. Al Weaver of Pratt & Whitney Engines, Roland Crandall of GE Engines, and Steve Pringnitz of Allied Signal met with us at their sites and shared their experience in containment issues. Dr. Thomas Havel of the US Army assisted us in accessing classified documents relating to advanced armor. Barrier materials were provided by William Evancho of Structural Laminates Company, Caroline Holtzmann of Spectra Performance Materials, Tadao Kuroki of Toyobo, Lynn Bell of Warwick Mills, and Phil Cunniff of the Army Natick Research and Development Center.

Mario Oyola operated the SRI gas gun facility, and Ken Stepleton was responsible for the high-speed photography.

TABLE OF CONTENTS

	Page
EXECUTIVE SUMMARY	ix
INTRODUCTION	1
DEPARTMENT OF DEFENSE ARMOR TECHNOLOGY	1
Armor Materials and Their Properties	1
Metals	3
Ceramics	6
Polymers	11
Composite Materials	13
Fiber-Reinforced Materials	17
Summary, Conclusions, and Prospects	17
Strategies for Defeating Military Projectiles	18
THE ENGINE FRAGMENT THREAT	21
Characteristics of Aircraft Engine Fragments	21
Critical Fragment-Vulnerable Areas on an Aircraft	23
FRAGMENT BARRIER DESIGN	24
Fuselage Wall Fortification	24
Local Protection of Control Lines and Fuel Lines	28
Fragment Barriers Within the Nacelle	28
Containment	29
FRAGMENT BARRIER EVALUATION	30
Impact Experiments	30
High-Strength Fabric Materials	37
Quasi-Static Tests and Redesign of Clamping Scheme	38
Impact Experiments—Single-Layer Targets	39
Penetration Mechanisms	43
Impact Experiments—Multiple-Layer Targets	43
Discussion and Conclusions	45
Finite Element Calculations	45

	Page
THE NEXT STEPS	49
Near-Term Engine Fragment Barriers	49
A Computational Design/Evaluation Capability	50
Computer Codes	50
Deformation and Failure Models	50
High Strain Rate Constitutive Data	51
High Strain Rate Test Techniques	51
Summary	51
CONCLUSION	51
Review of Military Armor Technology	51
Barrier Design for Engine Fragments	52
Fragment Barrier Test Facility	52
Computational Simulations	52
RECOMMENDATIONS	53
REFERENCES	54
APPENDIX A—INGRID AND DYNA3D INPUT FILES FOR THE FRAGMENT IMPACT CALCULATIONS	

LIST OF FIGURES

Figure		Page
1	Projectile Defeat Mechanisms	19
2	Hypothesized Fragment Energy Distribution Showing How Barriers of Increasing Energy Absorption Capability Truncate an Increasing Number of Fragments	22
3	Fuselage Wall With Interior Panel and Insulation Removed to Reveal Structure	25
4	Typical Fuselage Wall and Ballistically Reinforced Fuselage Wall	26
5	Fragment Barrier for Flight Control Line Protection	28
6	SRI Gas Gun Facility for Evaluating Potential Engine Fragment Barriers	31
7	Various Target Mounting and Clamping Schemes Used in Gas Gun Impact Tests to Evaluate Potential Engine Fragment Barriers	32
8	Representative Frames From High-Speed Camera for Two Fragment Impact Tests	35
9	Recovered 6-in.-Square Target Plates From Two Fragment Impact Tests	36
10	Kinetic Energy Absorbed by 6-in.-Square Targets During Impact by 25-Gram Fragment Simulator at 80 m/s	37
11	Views of UHMW Polyethylene Felt After Quasi-Static Deformation by Fragment Simulator	39
12	Kinetic Energy Absorbed by High-Strength Fabric Targets During Penetration by a 25-Gram Fragment Simulator at 80 m/s	41
13	Comparison of Kinetic Energy Absorbed By Rigid-Wall and Fabric Targets During Penetration by a 25-Gram Fragment Simulator at 80 m/s	42
14	Comparison of Energy Absorbed Per Unit Areal Density for Full Penetration by a 25-Gram Fragment Simulator at 80 m/s	42
15	Photos of Central Sections of Single-Ply Fabric Targets Recovered After Impact and Full Penetration by a 25-Gram Fragment Simulator at 80 m/s	44
16	DYNA3D Configuration for Fragment Simulator Calculations	47
17	DYNA3D Calculated Results for Test 3, Impact Velocity 59 m/s	47
18	DYNA3D Calculated Results for Test 6, Impact Velocity 95 m/s	48

LIST OF TABLES

Table		Page
1	Characteristics of Ceramic Materials Considered by ALCOA for Armor Applications	9
2	Properties of Candidate Ceramic Armor Materials Considered by DuPont	12
3	Properties of Selected High-Performance Fibers	14
4	Ceramic Matrix Composite Properties	15
5	Gas Gun Impact Tests Using Aircraft Skinlike Materials	34
6	High-Strength Fabric Materials Obtained for Impact Studies	38
7	Gas Gun Impact Tests Using High-Strength Fabric Materials	40
8	Material Properties Used in Finite Element Impact Simulations	46

EXECUTIVE SUMMARY

To enhance the survivability of commercial aircraft in the event of an uncontained turbine engine failure, the Federal Aviation Administration (FAA) is sponsoring a research program aimed at protecting components of the aircraft that are critical to continued safe flight and landing. As a member of the FAA contractor team, SRI International identified technology transfer opportunities for aircraft engine fragment barriers by surveying the recent advances in Department of Defense (DOD) armor structures. This survey included the mechanical properties, ballistic performance, and the material weight and cost of metallic alloys, ceramics, polymers, and composites.

SRI concluded that highly ordered, highly crystalline, high molecular weight polymers, because of their low density and high strength, hold great promise for engine fragment barriers on aircraft. Fibers of certain aramids, polyethylenes, and polybenzoxazole (PBO) appear capable of providing a useful measure of ballistic protection in the most weight-efficient manner.

The survey further showed that advanced ceramics should be considered as components in aircraft armor. In particular, encapsulated tiles of Al_2O_3 , SiC, B_4C , TiB_2 , AlN, and certain ceramic alloys and cermets were shown to be effective in defeating projectiles at areal densities significantly lower than their metallic counterparts.

For metals, although the strength and toughness of aluminum alloys, titanium alloys, and steels have been enhanced in recent years, gains in ballistic resistance have been only marginal. Nevertheless, these newer alloy variants may find application within the engine nacelle.

Based on the findings from the DOD armor review, a fragment barrier scheme was conceived for preventing low-energy fragments from penetrating the fuselage wall and then severing control lines or damaging a second engine. The scheme consists of fabrics and felts of high-strength polymer fibers. The added weight and cost are minimized by replacing existing materials in the fuselage wall with dual function ballistic materials. A second scheme uses an inclined laminate of polymer, ceramic, and metal alloy to provide local protection to fuel and control lines.

A fragment impact test facility was designed, constructed, and used to begin to evaluate the ballistic resistance of fuselage wall materials and several advanced materials. Against a 25-gram simulated fragment at 80 meters per second, glass fiber-aluminum laminates absorbed nearly twice the energy absorbed by conventional aluminum fuselage skin of equivalent weight. Strong polymer fibers, tested as layups and weaves, however, absorbed much higher energies and in terms of areal density were 4 1/2 to 15 times more efficient than aluminum fuselage skin, suggesting that these materials will perform well as components of aircraft fragment barriers.

A computational tool was developed for interpreting impact experiments and designing barriers. A tied-node-with-failure algorithm introduced into the material failure model used in the DYNA3D code enabled SRI to estimate the residual velocity of a penetrating fragment and thus evaluate the energy-absorbing capacity of potential barrier systems. Computed results on aluminum aircraft skin agreed well with experiments; more complex failure models and high-strain-rate material properties are needed to apply the tool to polymer fibers.

This work confirmed high-strength polymer fibers as the advanced material most appropriate for protecting aircraft from uncontained engine fragments and identified three polymers as having the prerequisite low density and high strength. Polybenzoxazole, because of its exceptional ballistic properties, flame resistance, and water absorption resistance, appears particularly suited as a barrier material. The next step is to design practical barriers from these fibers. Much design flexibility exists, because the three fiber types can be produced in many diameters, lengths, and surface finishes; the fibers can be configured in many types of weaves, felts, and layups; and these configurations can be assembled in many geometries, fiber mixes, and can include other materials.

Two efforts are recommended to capitalize on these findings: (1) a semiempirical effort to evaluate the ballistic effectiveness of existing polymer fabric structures and barrier designs and (2) an effort to develop a computational capability for designing and evaluating barrier schemes based on material failure mechanisms and properties. The former effort could result in acceptable barrier systems in the near term; the latter effort aims for the longer term design of barrier systems more optimal in terms of weight, cost, and ease of installation and removal for aircraft inspections. These efforts can be performed simultaneously.

INTRODUCTION

Over the years, several civil aircraft accidents having catastrophic consequences have resulted from damage to critical aircraft components by flying engine fragments produced by an in-flight engine failure. To reduce the probability of catastrophic consequences in possible future failures, Congress passed the Omnibus Reconciliation Act of 1990 (Public Law 101-508). This law resulted in the Aircraft Catastrophic Failure Prevention Research (ACFPR) Program and mandated the Federal Aviation Administration to develop and apply advanced technologies and methods for assessing, preventing, or mitigating catastrophic failures that can result in civil aircraft accidents. The ACFPR plan⁽¹⁾ considers the three main components affecting the safety of an aircraft: turbine engines, airframes, and flight controls. A systems approach is applied in the analysis of each component to address the interacting influence of all three components on aircraft safety and the cascading effect of single-point failures on other critical systems.

In support of this mandate, SRI International conducted a research program, under Federal Aviation Administration supervision, addressing protection against threats resulting from failures in turbine engines (Turbine Engine Failure Prevention Task III). The SRI objective was to review the rich body of armor technology held by the Department of Defense and to identify concepts, materials, and armor designs that could lead to practical barriers to engine fragments on commercial aircraft. This report describes the findings and suggests barrier designs for aircraft fragment protection.

DEPARTMENT OF DEFENSE ARMOR TECHNOLOGY

Department of Defense (DOD) efforts to develop improved armors for battle tanks have been ongoing for many years. Efforts were particularly intensive in the past decade, and substantial improvements were obtained through innovative protective strategies, advanced materials, and new armor configurations. The Defense Advanced Research Project Agency (DARPA)/Army/Marine Corps Armor/Anti-Armor Program⁽²⁾, initiated in January 1986 and completed in September 1993, resulted in significant technological advances that potentially can be exploited to mitigate effects of aircraft engine fragments. Although the DOD threats generally differ from the aircraft engine fragment threat in mass and velocity, the projectile defeat strategies, the advanced armor materials, and the barrier designs developed by DOD contractors are expected to be useful in developing improved turbine engine fragment barriers. This section briefly reviews traditional military armor technology and summarizes the findings of the recent advanced armor initiative with respect to advanced materials and projectile defeat strategies. In the following sections, we use these military insights to speculate on potential fragment barriers for civil transport aircraft.

ARMOR MATERIALS AND THEIR PROPERTIES.

The conventional medium carbon steel armor traditionally used on battle tanks today is often supplemented or supplanted by nonferrous materials such as aluminum and titanium, ceramics, polymers, and composite materials. The goal is to achieve the ballistic protection afforded by steel but at a reduced weight. Hence, these modern armor materials are of interest in the design of aircraft fragment barriers. This section reviews armor materials, starting with traditional armors and tracking the advances to present day.

A U.S. Army handbook of lightweight armor written by Mascianica⁽³⁾ is a useful reference for armor materials up to 1980. The handbook compiles ballistic information on the efficiency of various homogeneous and composite armor materials impacted by projectiles of various mass and velocity. Master ballistic performance curves are presented to show the effect of armor thickness or areal density, obliquity, projectile velocity, and environmental parameters.

Projectile diameters range from 0.022 to 4.8 inches and velocities range upward from 4000 feet per second; hence, the data are for lower mass and higher velocity projectiles than aircraft engine fragments (see Characteristics of Aircraft Engine Fragments). Nevertheless, the curves provide insight and an extrapolation basis that may be useful in designing engine fragment barriers. The handbook also includes ballistic data for heavier and slower fragments from grenades, mines, and shells filled with high explosives which are closer to engine fragment conditions.

The DARPA/Army/Marine Corps Armor/Anti-Armor (A/AA) Program⁽²⁾ was established upon recommendation by the Defense Science Board based on a study they conducted in 1985 that found a significant and alarming lag in U.S. armor and penetrator technology with regard to Soviet technology. The intent of the A/AA program was to create in the United States an armor industry similar to the existing electronics and aviation industries. Private companies, national laboratories, research institutes, and universities were encouraged to form teams and apply their technical strengths to develop and produce advanced armor systems. The military could then draw on the broad industrial technology base, as it has done in aircraft and electronics, for innovations in armor to upgrade the protection on combat vehicles. DARPA was tasked as the program manager, Los Alamos National Laboratory was tasked as product evaluator, and ALCOA, DuPont, FMC Corp. *, and Honeywell* were selected as prime contractors. Each prime contractor selected four to five organizations for their team.

The objective of the four competitive contractor teams was to innovate, design, and construct more efficient and effective armor systems for light and medium armored vehicles and heavy main battle tanks that could protect against current and future threats but under specified constraints of weight, space, and cost. Emphasis was placed on advanced materials of all classes (metals, ceramics, polymers, and composites) and innovative structures. The evolving systems of each contractor team were periodically evaluated by an independent agency, the Advanced Technology Assessment Center (ATAC) at Los Alamos National Laboratory (LANL). Each team was required to deliver its armor system to LANL for ballistic testing against specific kinetic and chemical energy warheads.

The program, which endured for more than 7 years from January 1986 until October 1993, was funded by DARPA at a total cost of more than \$60 million, and in-kind and dollar matching cost sharing by the participants roughly doubled this amount. Many new armor concepts and products resulted and several armor systems met the very demanding requirements for ballistic protection at acceptable weight and cost. Several products have been adopted by military services; some were implemented in Desert Storm.

It behooves the commercial aircraft industry to exploit this new knowledge to improve current barrier technology in commercial aircraft and reduce still further the risk of a catastrophic accident from in-flight engine failure. The sources of information for the more recent armor

*These companies are now known as United Defense and Alliant TechSystems, Inc., respectively.

materials are DOD technical reports, many of which are classified. Most of the reports from the A/AA program are classified as SECRET-National Security Information under the DARPA Classification Guide⁽⁴⁾ SCG-117. These reports are maintained in a library at the Armor Mechanics Branch of the Army Research Laboratory at Aberdeen Proving Ground, Maryland. The point of contact is Dr. Thomas A. Havel.⁽⁵⁾

Many of the materials that were considered for use in armor and their mechanical properties are unclassified [according to the newer Classification Guide-Armor Materials⁽⁶⁾ of 30 July 1993] and can be presented in this report. However, the ballistic performance of materials and structures are, in general, classified and, hence, must be discussed in qualitative terms. Where possible, relative rankings of materials are given in terms of their ballistic performance against specific unnamed projectiles to give the reader some guidance in designing aircraft barriers. The reader can refer to the original classified documents for more detail. In this report we discuss each class of material and give, as available, densities, costs, and relevant physical and mechanical properties of specific materials within each class.

METALS.

Steels. Since the inception of the American military, steels have been the material of choice for vehicle armor. Besides their effectiveness in defeating impacting projectiles, steels are inexpensive relative to other materials and are excellent structurally; being weldable, durable, formable, corrosion resistant, compatible with other structural components, and field repairable. For ballistic protection purposes, steel can be modified by compositional alterations and thermomechanical treatments to tailor strength, toughness, and hardness; allowing the armor to be adapted to a wide range of threats while simultaneously performing a structural function. Because of its wide use, steel is the standard against which all other armors are evaluated. The main drawback of steel is its high density, which results in heavy armor structures.

Much effort has been directed at metallurgical modifications to improve the ballistic performance of steel against various threats and much success has been achieved. Metallurgical research has shown that processing to produce super-clean steel results in enhanced strength and ductility and, consequently, improved ballistic properties. Steel plates with very hard surfaces are effective at deflecting, deforming, or fracturing projectiles. Dual hard plates consisting of a hard front plate and a tough backing plate, either strongly or weakly bonded to each other, are effective in defeating a projectile in two stages (breaking the projectile, then absorbing the energy of the fragments). Multilayer laminates resist propagation of cracks and shear bands, thereby resisting plugging. High carbon tool steels were considered for armor because of their high hardness and concomitant tendency to shatter impacting projectiles. Teams in the A/AA program performed ballistic tests on tool steel plates and on plates encapsulated in aluminum. The intent was that tool steel should function as a "tough ceramic." However, tool steels had a lower ballistic limit than Coors AD-90 alumina in a similar encapsulated target configuration and under similar projectile conditions.

Improvements on conventional dual hardness steel armor were obtained using an ultrahigh carbon steel as the front layer and roll bonding it to a conventional rolled homogeneous steel. The ultrahigh carbon steel (UHCS) contained 1% to 2% carbon (a composition between tool steels and cast iron not currently available commercially, but easily produced) in the form of

carbides kept small and distributed in the microstructure by continuous hot working during shaping. In this condition, the UHCS could be roll bonded to the softer backing steel, and the strength of the interface could be tailored from very weak to very strong. A final heat treatment resulted in a front layer hardness of R_c 68, several points harder than previous dual hard armor. This armor outperformed other dual hard armors, and UHCS multilayer laminates outperformed UHCS dual hard armors. Ultrahigh carbon steels, developed by Sherby at Stanford University⁽⁷⁾ and then further by SRI,⁽⁸⁾ were evaluated for the Honeywell armor package.⁽⁹⁾

For ballistic protection in aircraft applications, steels and most other metallic alloys are unattractive because of their high densities. However, in engine structures where high-temperature strength is required, steels and other alloys are used as containment structures within nacelles.

Several attempts by the DOD community to design steel armor structures to improve the performance-to-weight ratio have met with some success. For example, the ALCOA team⁽¹⁰⁾ showed that perforated armor (steel plate containing a pattern of through holes) was more effective than monolithic plate. In another design variation, P900 440 stainless steel plates containing a closely spaced array of ceramic rods were shown to suffer a smaller area of damage when attacked by a projectile, thereby having better multihit capacity.⁽¹⁰⁾ Such limitation of damage area is desirable in containment considerations, where it is important to prevent engine debris from exiting the nacelle through a hole produced by a large disk section.

Steels also found use as encapsulation materials for ceramic plates, as explained later in this section, allowing ceramic armor to perform more effectively by inhibiting the dispersion of ceramic fragments from the path of the penetrator.

Aluminum Alloys. Military interest in aluminum as an armor material dates back at least to World War II when plates of 2024-T4 and 7075-T6 were tested against armor-piercing ammunition and fragments from explosive-filled shells. Research to improve ballistic properties began after the war and consisted of composition modifications, improved cleanliness, and thermomechanical treatments. The results were the strain-hardened alloys 5083 and 5456, which had superior cracking resistance and, in the H321 temper, were less susceptible to stress corrosion. Later, the precipitation-hardened Al-Zn-Mg 7039 alloy was developed, which has higher strength and provides greater ballistic protection than the 5083 alloy. The 7039 alloy, however, is less ductile and is likely to produce back-surface spall when attacked by fragments from an exploding shell.

With a density roughly one-third that of steel, aluminum alloys are of major interest as aircraft armor. Certain alloys provide better ballistic protection than the standard aircraft fuselage alloy (2024 in the T3 and T351 condition) and wing alloy (7075-T651 and 7178-T651), but the gains are small. Traditional armor aluminums such as 7039-T64 and 5083-H131 have ballistic limits only slightly above current aircraft structural alloys. Higher strength and higher toughness alloys such as 2524-T3 for the Boeing 737 fuselage and 2325-T39, 2224-T3511, 7150, and 7055 for the lower and upper wings are replacing the standard alloys on all Boeing models but provide only marginally better impact resistance. The ALCOA A/AA team found that ballistic performance improved with increased strength but not significantly. Texture changes in 2519 aluminum armor plate produced no enhancement in ballistic performance.⁽¹⁰⁾

Aluminum alloy plate stock and wrought 206 aluminum were used as confinement plates for hard tiles of ceramic and tool steel. Confined ceramic armor blocks were also produced by squeeze casting. In an earlier armor development program, Reynolds Aluminum investigated the feasibility of several alloys and processing techniques for encasing ceramic blocks.⁽¹¹⁾ The castable aluminum alloy 535Q outperformed 5083 and 7039 sheet alloys as well as castable alloys A356, A206, and 772.

Magnesium Alloys. Magnesium-lithium alloys are significantly less dense than aluminum alloys and thus hold appeal as potential armor materials for aircraft. Ballistic evaluation of the Mg-13%Li-6%Al showed good performance against small arms and fragments. However, because of its high ductility, low hardness, and stress corrosion susceptibility, this alloy was deemed unsuitable for structural functions and has not been pursued for armor applications.

Titanium Alloys. Early titanium alloys were found to be excessively brittle in ballistic tests, but because of their low density relative to steel, the Army let contracts in the mid-1950s aimed at developing titanium alloys with enhanced performance. This work resulted in Ti-6Al-4V, which is the most widely used structural titanium alloy as well as the titanium armor alloy of choice. Other titanium alloys have been evaluated ballistically over the years but show no improvement over Ti-6Al-4V. A variation known as 62S and the high-strength beta alloy 15-3-3-3 provide a good balance between ballistic performance and structural strength.

Fanning⁽¹²⁾ recently investigated the ballistic performance of TIMETAL 62S, a low-cost variation of Ti-6Al-4V, against .30 and .50 caliber ball and fragment-simulating projectiles. The alloy performed better than Ti-6Al-4V for plate thicknesses greater than the projectile diameter but poorer than Ti-6Al-4V for thinner plates. Such results are consistent with findings in steel and aluminum alloys which also showed that variations in composition and processing produce only small changes in ballistic performance and that ballistic performance strongly depends on projectile characteristics.⁽¹²⁾ Alloys with ultimate tensile strengths less than 120 ksi, however, are not susceptible to brittle cracking and back surface spall. Brittleness is suppressed in titanium alloys by keeping interstitial impurities of oxygen, carbon, nitrogen, and hydrogen in low concentrations.

Starting with cross-rolled Ti-6Al-4V stock, FMC⁽¹³⁾ experimented with forging conditions and identified a condition that produced the material with the highest ballistic resistance. The resulting heavy plates had mass efficiencies 50% higher than rolled homogeneous steel armor and consequently were used for the hatch on the Bradley fighting vehicle.

Of the A/AA teams, only FMC used titanium alloys in its ground vehicle armor designs, and then only sparingly. Nevertheless, titanium alloys offer high strength-to-weight ratios at an attractive toughness level and thus should not be discounted as aircraft armor. Indeed, titanium alloys may be the best suited materials in high-performance military aircraft, where both protective and structural performance are required, tare weight is limited, and cost considerations are secondary. Costs per pound of three titanium alloys, based on a 3,000-lb minimum order, are given below:⁽¹²⁾

Thickness (inch)	TIMETAL [®] 6-4	TIMETAL [®] 62S	TIMETAL [®] 15-3
0.030	\$48	\$46	\$34
1	\$16	\$14	N/A

CERAMICS. It was known since the 1970s that ceramics make good armor and in many instances outperform conventional rolled homogeneous steel armor. High compressive strength allows ceramics to exert large stresses on impacting projectiles, stresses that act to deform, deflect, and fracture the projectile. In the cases of thick, encased ceramic tiles and blocks used in heavy armor for main battle tanks, projectiles were defeated by the erosive action of ceramic particles as the penetrator advanced into the block. Encasement also provides increased multihit protection. Typical densities of ceramics are 3 to 4 g/cm³, significantly less than most metals (except for aluminum) and second as a class only to polymers, qualifying ceramics as potential materials for ballistic protection on aircraft. A disadvantage of ceramics is their high cost relative to metals.

The use of ceramics as armor materials was driven by the need in military aircraft to protect the pilot and critical aircraft components from attack by small-caliber ball and steel-cored ammunition. Weight constraints precluded standard steel armor and metallic/fabric sandwich plates. Instead, composite hard-faced armors consisting of ceramic backed by resin-bonded fiberglass or Kevlar were developed that provided the required ballistic protection within the 10 lb/ft² prescribed maximum areal density. Today, many of the military helicopters and other low-speed aircraft are equipped with ceramic component armor. Generally speaking, ceramic component armors are superior to other armors for shell protection at areal densities between 5 and 12 lb/ft²; at lower densities, however, performance degrades and other armors may be better. Thin ceramic tiles are incorporated into protective vests to shield against rifle and high-power handgun projectiles.

The understanding of how ceramics defeat projectiles and the conditions that enhance ceramic armor performance were summarized by the ALCOA Team⁽¹⁰⁾ as follows.

“Ceramic materials as components in armor systems have been investigated by a number of groups. Viechnicki et al.⁽¹⁴⁾ published relative ballistic merit ratings based on V₅₀ limits on one-inch-thick TiB₂, SiC, B₄C, and Al₂O₃ tiles against a variety of threats. These workers reported that the best TiB₂, SiC, and B₄C performed equally well, while the best alumina had a relative merit rating of 80% of these other materials. They found no clear relationships between ballistic performance and other ceramic properties; although they suggested that if one property had to be used as a predictor of ballistic performance, it would be hardness. These workers also concluded that multiphase and composite ceramics such as 25% SiC/75% Al₂O₃, 10% SiC/90% TiB₂, and 10% TiC/90% TiB₂ perform poorer than purer monolithic ceramics containing minimal amounts of second phases. In an extension of the MTL work on ceramic composites, Kliman and Slavin⁽¹⁵⁾ reported that the ballistic performance of a sintered alpha SiC doped with from 5-30 vol% TiB₂ degraded with increasing TiB₂ content.

Landingham and Casey⁽¹⁶⁾ reported the ballistic performances of a wide variety of materials, and if their data is reduced to V_{BL} divided by thickness of ceramic, they show that a cermet containing TiC and Ni-Mo has the highest value of any material used.

Ballistic performance is a complex synergistic function not only of the material properties but also the geometries and amounts of materials in both the threat and target. Wilkins et al.⁽¹⁷⁾ showed that ceramic tiles ballistically perform well against a simulated 7.62 mm projectile only when they are backed by a stiff backup plate. Wilkins⁽¹⁸⁾ showed that over a wide range, the ballistic limit velocities for a ceramic-faced aluminum target increase nonlinearly with ceramic thickness. Mayseless et al.⁽¹⁹⁾, using a 12.7 mm hard-steel projectile, verified this nonlinearity for ceramic targets containing no backup material. Yasiv et al.⁽²⁰⁾, using a 14.5 mm BS41 round, claimed that at low projectile velocities, ceramic target efficiencies decrease rapidly because the speed of the waves traveling through the ceramic is independent of impact velocity and fracture occurs at very early times during the traverse of the projectile. These workers also showed evidence that ceramic/aluminum targets performed best when shot at zero degrees obliquity. They also suggested that the width-to-thickness ratio of the target materials be 10:1 so that the fracture conoid has time to form before transverse waves are reflected from the edges of the target.

Both Wilkins and Mayseless et al. observed that, for a given ceramic thickness, the ballistic limit increases linearly with increasing backup plate thickness. At some point, an abrupt increase in ballistic limit in the curve occurs, and it then continues in a linear fashion. Wilkins et al. stated that this “kink” occurs when the thickness of the backup plate reaches the diameter of the projectile. However, Mayseless et al. showed that the kink they observed occurred at the same backing thickness as Wilkins despite the difference in caliber and further stated that the kink was not observed for ceramic widths under some unspecified value. Yasiv et al. claimed that at a ratio of ceramic thickness to backplate thickness of 1.33 the weight of targets will be at an optimum for ceramic-faced aluminum targets. These workers further reported that changes in the adhesives used to bond the ceramics to the backup plate did not affect the mass efficiencies of the targets, but when silicon grease was used instead of the adhesives, the mass efficiencies decreased. Mayseless et al. also found that the addition of a nonceramic face plate in front of the ceramic decreased the ballistic limit of the target.

Mayseless et al. also attempted to deal with scaling factors which might be applied to armor design against threats of differing masses traveling at different velocities at differing thicknesses of ceramic. Their results may be expressed in the following equations:

- [1] $v_2/v_1 = (m_1/m_2)(h_2/h_1) = k$, for no or very thin backup plates,
- [2] $v_2/v_1 = k^{(1/2)}$, for a backup plate thickness near the kink, and
- [3] $v_2/v_1 = k^{(1/n)}$, for thicker backup plates.

In these equations, v 's and m 's are velocities and masses of projectiles, respectively, h 's are thicknesses of ceramic, and subscripts 1 and 2 correspond to cases 1 and 2.

To summarize, previous work suggests that increasing the ratio of the elastic impedance or yield strength of the target to the penetrator and increasing the time that these target properties are retained will result in a better performing armor. Fracture toughness of the target, which is generally low for ceramics, combined with high elastic impedance should be increased if the armor is to be improved. In a multicomponent target, the ceramic can be made more effective by supporting it with a stiff backing that can mitigate or resist tensile wave fracture and confining it so that when fracture occurs there remains sufficient material in the penetrator path to stop its movement.”

Ceramic materials, because of their high hardness and abrasiveness relative to metals, attracted the attention of every A/AA team. Five basic ceramics were identified as candidates for armor— Al_2O_3 , SiC , B_4C , TiB_2 , and AlN . Each ceramic has many subgrades, distinguished by variations in composition and processing conditions. A number of ceramic “alloys” were made by mixing and consolidating powders of two or more ceramics and were evaluated for their armor potential. However, the ballistic performances of subgrades and alloys of a ceramic did not in any case exceed that of the base ceramic by more than 25%.

The ALCOA team evaluated 30 ceramic materials. The ballistic performance of each of the ceramic materials was evaluated against three threats and each material was characterized by vendor, process, density, porosity (%), average grain size, four-point-bend strength, elastic modulus, sonic velocity, elastic impedance, fracture toughness, and microhardness. Heiple and Kornish⁽¹⁰⁾ described their results as follows:

“One result of the work was the discovery of a multiphase TiB_2/SiC composite, identified as TSA-3, which gave a target mass efficiency 22 percent higher than the target mass efficiency for hot pressed TiB_2 against the 14.5-mm BS41 projectile. Ranking of mass efficiencies for the highest performing ten ceramic materials versus the 14.5-mm BS41 projectile were: TSA-3 > hot pressed TiB_2 > sintered TiB_2 > hot pressed SiC > hot pressed TiB_2/AlN laminate > sintered alpha SiC > hot pressed Al_2O_3 > hot pressed A•B ($\text{Al}_2\text{O}_3/\text{B}_4\text{C}$ multiphase composite) > hot pressed AlN > sintered Hexaloy ST (TiB_2/SiC multiphase composite). Microstructural and mechanical data suggested that ceramic microcomposites can ballistically outperform monolithic ceramics if the bonding between the matrix and minority phases is strong and if the minority phase forms large agglomerates during processing. Hot pressing produces superior ballistic ceramics, but if the ceramic powder used is pure and fine grained, pressed and sintered parts may have mass efficiencies within 18 percent of hot pressed parts.”

Table 1 lists the ceramics materials tested by the ALCOA team, the processes by which they were produced, the producers, and properties that were believed to be relevant and could easily be measured.

TABLE 1. CHARACTERISTICS OF CERAMIC MATERIALS CONSIDERED BY ALCOA FOR ARMOR APPLICATIONS

Material	Vendor	Process	Thick (in.)	Density (g/cm ³)	Percent Porosity	Avg. Grain Size (μm)	4-pt Strength (psi)	Elastic Mod (psi)	Sonic Vel. (m/s)	Elastic Impedance (x10 kg m ² s ⁻¹)	K _{IC} (MPa√M)	Micro-hardness (kg/mm ²)
AlN	Cercom	Hot press	1.00	3.27	0.38	3.34	54899	46.5 x 10 ⁶	9906	3.24	3.48	1091.00
Al ₂ O ₃	Cercom	Hot press	0.80	3.98	0.04	1.16	63972	56.7 x 10 ⁶	9880	3.93	3.21	2024.00
Al ₂ O ₃	Alcoa	Sintered	0.80	3.93	0.18	1.09	53175	54.5 x 10 ⁶	9857	3.87	4.50	1699.00
Al ₂ O ₃ , 92	Ceraver	Sintered	0.97	3.66	0.56	3.73	49445	44.5 x 10 ⁶	9150	3.35	4.50	893.62
Al ₂ O ₃ , 94	Ceraver	Sintered	0.99	3.71	0.16	1.84	42757	43.3 x 10 ⁶	8984	3.33	4.07	1032.48
Al ₂ O ₃ , 87	Pakco	Sintered	0.80	3.43	0.05	1.79	28495	34.4 x 10 ⁶	8300	2.85	3.10	800.00
Al ₂ O ₃ , 96	Pakco	Sintered	0.80	3.71	0.16	2.17	37899	44.9 x 10 ⁶	9138	3.39	3.40	1126.00
Al ₂ O ₃	Coors	Sintered	0.85	3.60	0.12	1.59	56100	39.6 x 10 ⁶	8707	3.13	3.08	1105.00
Al ₂ O ₃ , 99.5	Coors	Sintered	1.00	3.88	0.37	7.00	53091	40.46 x 10 ⁶	2650	1.05	4.65	1449.00
B ₄ C	Eagle Picher	Hot press	1.00	2.51	0.23	NA	55653	63.6 x 10 ⁶	13209	3.35	4.89	4175.48
B ₄ C	Eagle Picher	Hot press	1.20	2.51	0.23	NA	55652	63.6 x 10 ⁶	13209	3.35	4.89	4175.00
B ₄ C	Cercom	Hot press	1.20	2.51	0.23	NA	53910	65.8 x 10 ⁶	13434	3.37	4.15	4128.33
Sialon	Alcoa	Sintered	1.00	3.22	0.38	NA	68682	83.3 x 10 ⁶	13363	4.30	4.00	1516.41
Sialon HP	Alcoa	Sintered	1.00	3.23	0.96	NA	49137	85.8 x 10 ⁶	13464	4.35	4.15	1498.60
Sialon	Kenametal	Sintered	1.00	3.24	0.00	NA	78476	45.8 x 10 ⁶	9844	3.19	6.09	1729.56
Sialon 3.5	Alcoa	Sintered	1.00	3.24	0.57	NA	33241	68.1 x 10 ⁶	12004	3.89	3.72	1223.68
Alpha Sialon	Alcoa	Sintered	1.00	3.21	0.38	NA	66289	85.2 x 10 ⁶	13492	4.33	4.13	1479.62

TABLE 1. CHARACTERISTICS OF CERAMIC MATERIALS CONSIDERED BY ALCOA FOR ARMOR APPLICATIONS (CONCLUDED)

Material	Vendor	Process	Thick (in.)	Density (g/cm ³)	Percent Porosity	Avg. Grain Size (μm)	4-pt Strength (psi)	Elastic Mod (psi)	Sonic Vel. (m/s)	Elastic Impedance (x10 kg m ² s ⁻¹)	K _{1c} (MPa√M)	Micro-hardness (kg/mm ²)
SiC FG	Alcoa	Sintered	1.00	3.13	1.25	2.09	43329	60.3 x 10 ⁶	11910.00	3.73	4.00	3190.14
SiC CG	Alcoa	Sintered	1.00	3.17	0.12	1.71	40559	61.9 x 10 ⁶	12305.00	3.90	3.90	2845.54
SiC	Eagle Picher	Hot press	1.00	3.16	0.23	1.56	38044	61.6 x 10 ⁶	11595.00	3.66	2.44	2549.70
SiC (alpha)	Carborundum	Sintered	1.00	3.14	0.00	3.15	52667	60.6 x 10 ⁶	11501.00	3.61	2.46	2642.25
SiC	Ibiden	Sintered	1.00	3.02	0.05	1.51	48875	54.7 x 10 ⁶	11173.00	3.87	2.99	2777.54
TiB ₂ FG	Alcoa	Sintered	0.70	4.50	0.00	3.15	43739	83.3 x 10 ⁶	11298.00	5.08	4.80	2081.31
TiB ₂	Eagle Picher	Hot press	0.70	4.50	0.00	2.01	34518	82.5 x 10 ⁶	12407.00	5.58	5.72	2340.85
Al ₂ O ₃ /ZrO ₂	B&W	Sintered	1.00	3.94	1.41	2.95	34319	66.6 x 10 ⁶	10793.00	4.25	4.31	2302.62
A•B	Greenleaf	Hot press	1.00	3.17	0.19	1.57	65334	47.6 x 10 ⁶	10192.00	3.23	5.12	1926.40
Sialon/ZrO ₂	Alcoa	Sintered	1.00	3.25	0.35	NA	58793	55.0 x 10 ⁶	10799.00	3.51	5.50	1656.73
TiB ₂ /B ₄ C	Textron	Hot press	1.00	3.09	0.00	NA	62517	72.4 x 10 ⁶	12708.00	3.93	5.94	4265.78
TiB ₂ /SiC	Textron	Hot press	1.00	3.59	0.76	3.50	60523	75.3 x 10 ⁶	11750.00	4.21	5.21	2768.32
Al ₂ O ₃ /ZrO ₂	Cercom	Hot press	1.00	3.95	1.16	1.96	47262	56.8 x 10 ⁶	10000.00	3.95	4.89	1625.11
TSA-3	Alcoa	Hot press	0.70	3.57	0.05	NA	63774	72.7 x 10 ⁶	11847.00	4.23	6.57	2740.08
Hexaloy	Carborundum	Sintered	1.00	3.33	1.05	NA	50576	63.4 x 10 ⁶	11452.00	3.89	7.73	3151.75
B ₄ C/Al	Greenleaf	Infiltrate	1.00	2.58	2.95	NA	NA	11.2 x 10 ⁶	5469.60	1.61	NA	2024.19
A•B	Cercom	Hot press	1.00	3.19	0.05	NA	61474	61.7 x 10 ⁶	11540.00	3.68	9.23	2893.17

The DuPont team⁽²¹⁾ performed ballistic tests to rank 15 candidate armor ceramics according to their ability to defeat certain projectiles and found the rankings to vary depending on screening geometries and projectile characteristics. The team meticulously characterized the mechanical and microstructural properties of the materials and attempted to correlate the results with ballistic performance. However, no correlation could be established. Working as a DuPont subcontractor, GTE staff⁽²¹⁾ carefully and painstakingly examined and described the microstructure of each of the materials and performed fractographic investigations of failed strength specimens. Fracture toughness, strength, and microhardness, measured by several types of tests, are given in table 2 along with other characterization parameters.

The relatively high cost of ceramic plates often precludes their use in certain armor applications.⁽²²⁾ However, some studies show that ceramic plates made from low-cost starting materials perform as well as high-cost ceramics.⁽²³⁾ In particular, an inexpensive alumina provided ballistic protection equivalent to a sintered alpha-silicon carbide.

POLYMERS. Development of polymeric armor was driven initially by the desire in World War II to reduce the weight and increase the wearability of metallic body armor. The first nonmetal product was a vest made of Doron, a unidirectional glass fabric bonded with 20 to 25 wt% of a thermosetting polyester resin, developed in a joint Army-Navy effort. Later, vests made of a 12-layer nylon fabric were used by foot soldiers in the Korean conflict to protect against small, low-velocity shell fragments. Nylon fabric was also used as helmet liners, protective blankets, and frontal spall suppressors for ceramic composite armor.

The advent of high-strength aramids in the late 1960s permitted protective apparel with substantially better ballistic protection and wearability, and body armor made of Kevlar (a registered trade name of DuPont) became the norm. Today, aramid fibers are also produced by AKZO Industrial Fibers (Twaron[®]) and Teijin Limited of Japan (Technora[®]). In the 1980s still stronger fibers made of polyethylene were synthesized and opened the door for still higher-performance body armor. The polyethylene, marketed under the trade names of Spectra (Allied Signal), Dyneema[®] (by DSM of the Netherlands), and Tekmilon[®] (by Mitsui Petro Chemical of Japan) is one-third less dense than Kevlar and has already taken over a substantial share of the body armor market. Also in the mid-1980s, a still stronger and higher modulus fiber, polybenzoxazole (PBO), was invented at SRI International.⁽²⁴⁾ The PBO fiber will be produced commercially beginning in October 1998 by the Japanese chemical company, Toyobo, and will be marketed as Zylon.

Generally speaking (and bearing in mind that the ballistic resistance of a material depends on threat characteristics such as shape, mass, and velocity) fabrics and layups of polymeric fibers are competitive with metals and superior to ceramics at areal densities up to about 2 to 2.5 lb/ft². High-strength, high-modulus aramid and ultrahigh molecular weight polyethylene fibers configured in the form of mats, weaves, layups, cast sheet, or as reinforcements for organic, ceramic, or metallic matrices found application in advanced armors as spall shields and as encasement wrappings for ceramic tiles. Their low densities, 1.5 and 1 g/cm³, respectively, make these materials particularly attractive for aircraft barriers, where significant penalties are paid for weight. A disadvantage is their typically high cost: Kevlar fibers sell for \$12 to \$24 per pound; Spectra fiber products cost \$11 to \$35 per pound. As these fibers find other applications such as

TABLE 2. PROPERTIES OF CANDIDATE CERAMIC ARMOR MATERIALS CONSIDERED BY DuPONT

Material	Poisson's Ratio	Young's Modulus (GPa)	Shear Modulus (GPa)	Bulk Modulus (GPa)	Longit. Wave Vel (km s ⁻¹)	Trans. Wave Vel (km s ⁻¹)	Density (g cm ⁻³)	Elastic Impedance (kg mm ⁻² s ⁻¹)	Tensile Strength (MPa)	Compressive Strength (MPa)	Fracture Toughness (MPa√m)	Vickers Hardness (1 kg GPa)
TiB ₂	0.105	556	249	233	11.21	7.44	4.475	50.17	325	4601	—	19.51
TiB ₂ /TiC/Ni	0.128	498	220	223	10.62	6.94	4.569	48.54	—	5270	—	19.61
B ₄ C	0.166	445	190	221	13.70	8.67	2.514	34.45	210	6969	2.95	28.51
SiC	0.160	424	182	208	11.92	7.58	3.170	37.77	196	5433	2.46	22.96
Al ₂ O ₃	0.233	404	167	251	10.86	6.42	3.975	43.15	275	6619	3.21	17.70
Al ₂ O ₃ /SiCw	0.222	399	164	239	11.07	6.62	3.715	41.13	390	5619	4.89	19.75
TiN/β Si ₃ N ₄	0.249	364	145	242	10.09	5.83	4.275	43.12	470	5504	5.41	12.90
TiC/MoC/Ni	0.199	339	140	186	8.33	5.10	5.388	44.90	—	5243	4.73	14.38
α SiAlON	0.254	328	130	220	10.95	6.29	3.272	35.83	259	5577	4.21	17.81
α/12H SiAlON	0.255	316	126	215	10.78	6.18	3.280	35.37	279	6251	4.37	17.43
α/27R SiAlON	0.255	317	126	216	10.70	6.14	3.342	35.77	312	5937	5.10	16.57
β Si ₃ N ₄ A	0.277	309	121	232	10.99	6.10	3.257	35.78	537	5924	6.92	13.13
β Si ₃ N ₄ C	0.271	306	120	225	10.88	6.07	3.249	35.34	466	5726	7.18	12.92
β SiAlON	0.278	304	119	228	10.90	6.05	3.248	35.42	243	6020	3.51	13.73
TZP/Al ₂ O ₃	0.292	259	100	208	7.86	4.26	5.506	43.30	—	6164	4.77	14.74

GTE PRODUCTS CORPORATION
 CHEMICAL AND METALLURGICAL DIVISION
 GTE SUPPORT FOR THE DuPONT ARMOR BLUE TEAM

ropes and cables and reinforcement fibers for tires and composites, production capacity will increase, and the costs of fibers will fall. The mechanical and physical properties of several strong fibers are given in table 3.

The National Materials Advisory Board is conducting a study sponsored by the U.S. Navy, U.S. Air Force, Defense Advanced Research Projects Agency, and NASA to characterize the status of carbon and organic fiber science and technology as well as industry capability.⁽²⁵⁾ Yang⁽²⁶⁾ discusses and compares the properties of strong fibers in his recent book.

Aramid fibers, which consist of long chain synthetic polyamide molecules, retain their excellent mechanical properties up to 300°C. The low melting point of ultrahigh molecular weight polyethylene (147°C) prevents its use in elevated temperature applications and limits its incorporation into matrix materials to produce reinforced composites. Ballistic properties of the fiber are claimed not to deteriorate below 120°C.

The PBZ polymers first synthesized at SRI International⁽²⁴⁾ are thermally stable to 600°C and are the highest strength polymers yet developed. These heterocyclic rigid chain materials include variations known as PBT, PBO, and AB PBO and require very long and complex synthesis conditions. At present, they are available only in small quantity. Production and sales rights are now owned by Toyobo, a Japanese company that is working to develop large-scale polymerization and spinning processes to achieve economical production of the fibers. Commercial availability is expected in 1998. The fibers are expected to sell for about \$45 per pound.⁽²⁷⁾

COMPOSITE MATERIALS. Better armors can be achieved by combining two or more materials. Such composite materials take many forms—alloys and mixtures, particulate and fiber reinforced matrices, and spaced plates and multilaminates. Several of these composite materials are discussed in the following paragraphs.

Cermets. Cermets are mixtures of ceramic and metal that are attempts to obtain a combination of the desirable properties of both components. In hopes of producing materials with better ballistic properties than either ceramics or metals or producing similar ballistic properties at lower areal densities, the A/AA teams evaluated available cermets and in some cases synthesized new cermets.

The Lanxide Corporation*, which produces several aluminum-based cermets on a production scale for armor applications and applications of pumps and valves, produced several experimental cermets for the Honeywell and DuPont teams. The Lanxide PCS armor concept was selected for use in DuPont's light/medium armor. The DuPont team also attempted to manipulate the microstructure of a TiB₂/Ni cermet to enhance ballistic performance. Properties for the TiC/MoC/Ni and the TiB₂/TiC/Ni cermets are given in table 2.

* Lanxide Armor Products, Inc., 1300 Marrows Road, P.O. Box 6077, Newark, DE 19714-6077.

TABLE 3. PROPERTIES OF SELECTED HIGH-PERFORMANCE FIBERS

Fiber Type	Density (g/cc)	Strength [gpd (GPa) ^a]	Elongation (%)	Modulus [gpd (GPa) ^a]	Specific Strength (10 ⁶ in.) ^b	Specific Modulus (10 ⁸ in.) ^c	Fiber Diameter (μm)	Maximum Use Temperature (°C)
Kevlar 29	1.43	23 (2.9)	3.6	550 (70)	8.8	2.1	12	250
Kevlar 49	1.45	23 (2.9)	2.8	950 (135)	8.8	3.6	12	250
Kevlar 119	1.44	24 (3.1)	4.4	430 (55)	9.2	1.6	12	250
Kevlar 129	1.45	26.5 (3.4)	3.3	780 (99)	10.1	3.0	12	250
Kevlar 149	1.47	18 (2.3)	1.5	1100 (143)	6.9	4.2	12	250
Nomex	1.38	5 (0.6)	22	140 (17)	1.9	0.5		250
Technora	1.39	27 (3.3)	4.3	570 (70)	10.3	2.2	12	250
Ekonel	1.4	31 (3.8)	2.6	1100 (136)	11.8	4.2		150
Vectran	1.47	25 (3.2)		700 (91)	9.6	2.7		150
PBI	1.43	3.1 (0.4)	30	45 (5.7)	1.2	0.2		250
PBT	1.57	25 (3.5)	1.3	2690 (373)	9.6	10.3		350
PBO	1.57	24.6 (3.4)		2930 (406)	9.4	11.2		350
AB PBO	1.44	24.6 (3.1)		2430 (309)	9.4	9.2		350
Spectra 900	0.97	30 (2.6)	3.5	1400 (120)	11.5	5.3	38	100
Spectra 1000	0.97	35 (3.0)	2.7	2000 (171)	13.4	7.6	28	100
Thornel P55 Med M	1.8	10.8 (1.7)		1940 (308)	4.1	7.4	4–8	500
Thornel P100 HM	1.96	10.8 (1.86)	0.38	3300 (517)	4.1	12.6	4–8	600
Celion 3000 HS	1.8	25 (4.0)	1.8	1440 (230)	9.6	5.5		500
Boron	2.5	11.6 (2.55)	1.0	1800 (400)	4.4	6.9	33–140	2000
SiC	2.8	16 (4.0)	0.6	1700 (420)	6.1	6.5	10–12	1300
Alumina	3.25	6.3 (1.8)	1.2	730 (210)	2.4	2.8	17	1200
Nextel	2.5	7.8 (1.72)	2	690 (152)	3.0	2.6	13	1200
E glass	2.55	11.6 (2.6)	3	320 (72)	4.4	1.2	5–25	350
S glass	2.48	21.9 (4.8)	5.3	390 (85)	8.4	1.5	5–15	300
Steel	7.8	11 (7.6)	4.8	220 (150)	4.2	0.8		500
Dacron	1.38	9.2 (1.1)	15	115 (14)	3.5	0.4	25	150
Nylon 66	1.14	9 (0.9)	19	50 (8)	3.4	0.2	25	150

^aGPa = gpd x density/11.33.

gpd = GPa x 11.33/density.

^bSpecific strength (in.) = tenacity (gpd) x 3.82 x 10⁵.

^cSpecific modulus (in.) = modulus (gpd) x 3.82 x 10⁵.

Source: H. H. Yang, reference 26

A ceramic-particle-reinforced metal matrix composite, PRIMEX™, is aluminum highly loaded with SiC particles and made by a pressureless metal infiltration process. PRIMEX™ has been found effective against long rod projectiles. The ceramic matrix composite, DIMOX™, consists primarily of SiC particles in an alumina matrix and is made by a directed metal oxidation process. DIMOX™ has been used for cockpit protection in the Air Force's C-130, C-141, and C-17 transport aircraft as well as for breast plates in body armor and protection upgrades in lightweight vehicles such as trucks and personnel carriers.⁽²⁸⁾ Its effectiveness in containing aircraft engine fragments has been investigated.⁽²⁹⁾ The composition and processing of both families of materials can be varied to obtain different ballistic performance; both can be made in a wide range of sizes and shapes that need no extensive finishing. Typical engineering properties of these two materials are given in table 4. Lanxide has an ongoing materials development effort.

TABLE 4. CERAMIC MATRIX COMPOSITE PROPERTIES

Typical Engineering Properties	DIMOX-AS™	DIMOX-HT™
Compressive strength	1115 MPa	2600 MPa
Modulus of rupture	147 MPa	280 MPa
Elastic modulus	351 GPa	340 GPa
Shear modulus	146 GPa	140 GPa
Poisson's ratio	0.20	0.22
Fracture toughness	5.8 MPa-m ^{1/2}	4.6 MPa-m ^{1/2}
Thermal conductivity	147 W/m-K	140 W/m-K
Coefficient of thermal expansion (25-1000°C)	5.1 x 10 ⁻⁶ /K	5.5 x 10 ⁻⁶ /K
Bulk density	3.29 g/cm ³	3.33 g/cm ³
Hardness (RA)	80	88

Source: Lanxide Armor Products, Inc., 1300 Marrows Road, P.O. Box 6077, Newark, DE 19714-6077.

Glass Laminates. To enhance the ballistic protection provided by windows in World War II military tanks, personnel carriers, and aircraft, two or more panels of glass were laminated with a thin layer of tough plastic. In the ensuing years many new transparent materials were investigated with regard to their value as a transparent, ballistically efficient window. Included are hard glasses, Pyrex® glasses, Pyroceram®, chemically tempered glasses, cast acrylics, biaxially stretched acrylics, polycarbonates, single-crystal aluminum oxide, polycrystalline magnesium oxide, and spinels. Best performing windows currently configure transparent materials so that a hard material is on the outside to damage the projectile and a tougher, shock-resistant material is on the inside to absorb kinetic energy and suppress fragmentation.

Commercially available polycarbonate laminates, such as General Electric's LEXGARD series^{*}, provide protection against impacting fragments. The tough polycarbonate resists spall and generates no splinters or shards from the rear surface of an impacted plate.

United Defense (formerly FMC) developed a transparent armor that combines the optical principle of reflecting surfaces with the armor protection of high hard steel.⁽³⁰⁾ An array of inclined steel louvers separated by glass provides an optical path for viewing but no unimpeded path for a projectile. At an areal density of 20 lb/ft², the armor defeats .30 caliber AP-M2 at muzzle velocity and provides multihit protection at 3-inch centers.

Strong Fibers. Classical composites made of strong fibers embedded in polymeric, metallic, or ceramic matrices have been considered for ballistic protection. Although they may be lightweight, they are expensive and ballistic performance is usually poor. In the A/AA program, fiber-reinforced plastics found use as spall shields, as substrates for hardened facings of steel or ceramic, and as wrappings for containment of ceramic armor tiles. Such composites most often consisted of S-2 glass fibers in flat composite laminates of thermoset polyester, epoxy, and phenolic resins.

Price was a consideration that precluded the use of many nonpolymeric fiber materials such as carbon, boron, silicon carbide, and alumina. These fibers have the high tensile strength and stiffness of the polymer fibers (see table 3) but in addition have high hardness and compressive strength (which makes them useful in composites) and excellent thermal stability (they can perform at much higher temperatures than polymers). Typical densities of 1.8 to 4 g/cm³ are, however, significantly higher than those of polymers.

Carbon fibers produced from polyacrylonitrile (PAN) by thermal decomposition and high-temperature processing have outstanding tensile modulus, tensile and compressive strengths, and are stable to 500°C. This combination of properties makes carbon fibers attractive as reinforcement for advanced composites. Fiber densities of 1.7 to 1.9 g/cm³ result in a typical weight savings of 30% to 40% over glass fibers, an important benefit in weight-sensitive structures. The large initial investment costs for production facilities and the involved processing procedures set the price for carbon fiber at roughly \$30 to \$40 per pound.⁽³¹⁾

Like carbon, boron fibers are produced by an expensive thermal procedure and have a high specific strength and stiffness. Their main application is in composites and the primary market for boron composites is the aerospace industry. Boron fibers at present sell for \$350 to \$400 per lb.⁽³¹⁾

In summary, several high-performance fibers have been recently developed and have proved effective in soft- and hard-armor applications. UHMW polyethylene fibers have high strength and stiffness and the lowest density but deteriorate and melt at relatively low temperatures. Carbon fibers have the best thermal stability, but their relatively high density results in only moderate specific strength and stiffness. The inherent brittleness of carbon results in low-impact energy absorption and has largely precluded its use in armor. Glass fibers, while also brittle, offer much better ballistic resistance, although at substantial weight penalty. Aramid fibers have a combination of thermal and mechanical properties that provides a useful

^{*} Lexgard Laminates, GE Plastics Structural Products, One Plastics Avenue, Pittsfield, MA 01201.

compromise. PBO fibers have even better thermal and mechanical properties but are not yet available in commercial quantities. Increasingly, advanced composites incorporate two or more fiber types to exploit the most attractive properties of each fiber type and to reduce material and processing costs.

FIBER-REINFORCED MATERIALS. Fiber-metal laminates show some promise for ballistic protection. An aluminum-glass, fiber-aluminum sandwich sheet manufactured under the trade name Glare 5[®] absorbs nearly twice as much energy than a sheet of 2024-T3 aluminum of equivalent areal density but is several times more expensive. Other woven or laid up fiber composites tend to fail by brittle cracking under impact loads and thus absorb little kinetic energy.

United Defense⁽³⁰⁾ is developing composite armored vehicles for the Army and simultaneously developing composite component retrofitting. Fibers of carbon, S-glass, and E2-glass are incorporated in various polymeric matrices. Processing conditions are sought that improve ballistic performance. VARDOM, a vacuum processing technique, is currently used to fabricate panels up to 1 inch thick.

A 0°, 90° crossply layup of unidirectional fibers of polyethylene or aramid in a resin matrix provides better ballistic protection than a woven fiber composite. Such sandwich composites are available from Spectra Performance Materials[†] under the trade names Spectra Shield and Gold Shield.

Metal matrix composites such as titanium alloys reinforced with unidirectional SiC fibers were not expected to show cost-effective enhanced ballistic protection and hence were not evaluated in the recent A/AA program.

However, composite materials in the sense of adjacent plates of dissimilar materials (such as a ceramic plate backed by a steel or polymer plate) were found quite effective in enhancing ballistic resistance and were used widely by each of the A/AA teams. We consider these composites as structural design configurations and discuss them in the section on fragment barrier design.

SUMMARY, CONCLUSIONS, AND PROSPECTS. The increasingly more stringent requirement to provide ballistic protection at minimum weight and cost has driven the search for lower weight and less expensive materials with better ballistic properties. This requirement has resulted in experimentation with materials of all classes and with combinations of the several material classes. Simultaneously, incremental improvements in armor alloys, an extensive characterization of ceramic materials, and large advances in high-strength polymer and inorganic fibers have been achieved. Advanced materials of all classes are finding use in armor systems of today. Each material class has certain attractive properties for defeating projectiles: none has total capability. Increasingly, several material classes are combined to produce protective structures.

[®] Registered Trademark of Structural Laminates Company, P.O. Box 388-P, New Kensington, PA 15068-1327.

[†] Spectra Performance Materials, P.O. Box 31, Petersburg, VA 23804.

With the exceptions of polymers and inorganic fibers, it appears that significant enhancements in ballistic performance of the materials available today will not be forthcoming. Metallic alloys and ceramic materials will be improved incrementally by alterations in composition, processing procedures, and cleanliness. Their cost may be reduced by more efficient production techniques and by increased demand.

However, the trend in high-performance fiber development witnessed in the past 30 years will most likely continue. Polymeric, metallic, ceramic, glass, and carbon fibers having ever improving mechanical and thermal properties will continue to be innovated, driven by market demands for composites, for advanced structures such as armor, and for electronic and medical applications. Near-term likelihoods for high-strength, high-modulus organic fibers are new aromatic polyimides and heterocyclic polymers, especially when formulated in rigid or semirigid chain structures.

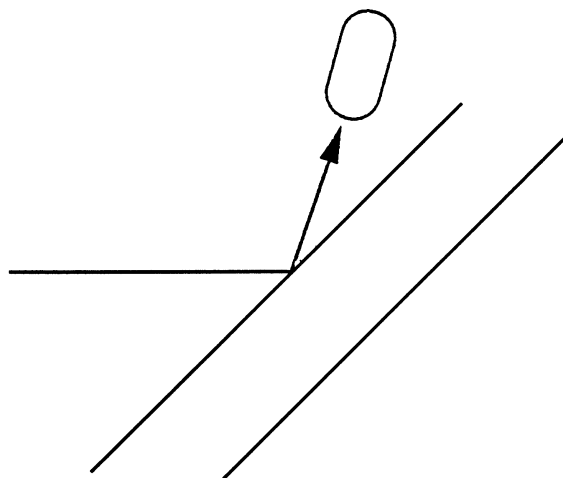
However, the DOD community realizes that advances in materials by themselves are inadequate for meeting the continual need for improved armor. This need must be addressed by clever barrier designs that incorporate several classes of material in a deliberate order to exploit the attractive ballistic properties of each. Thus, the burden for producing improved protective structures falls on the armor designer who, while keeping abreast of developments in materials, must devise projectile defeat strategies and configure the appropriate materials in the appropriate thicknesses, order, spacings, and angles to defeat the projectile at the most economical weight and cost. The following sections discuss projectile defeat strategies and armor structures that use advanced materials to implement those strategies.

STRATEGIES FOR DEFEATING MILITARY PROJECTILES.

The DOD contractor teams considered that the debilitating effects of impacting projectiles can be mitigated in several ways. These include deflecting the projectile, absorbing the projectile's energy by slowing or stopping it, deforming or fracturing the projectile, or eroding it as shown in figure 1.

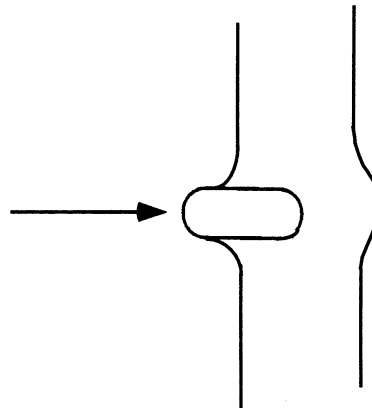
For example, the glacis (front end) of a battle tank is slanted with respect to the anticipated direction of projectile attack so that the threat will encounter an inclined surface and ricochet instead of penetrating, figure 1a. When the threat attacks at an angle of obliquity lower than required for ricochet, a thick plate of steel (typically rolled homogeneous armor, RHA) can absorb energy through plastic deformation as it is penetrated, thereby slowing or stopping the projectile, figure 1b.

In other cases the projectile may be deformed or fractured by an armor that is harder than the projectile. An example is hard steel such as quenched and tempered 4340. A deformed projectile loses its penetration power by presenting a larger impact area (hence, exerting a lower stress) on the target; a fractured projectile loses penetrability by virtue of lower mass and distributed load on target, figure 1c. Ceramic armors consisting of a block of ceramic tightly encased in steel (or aluminum or a strong fiber wrap) defeat projectiles by eroding the leading edge until a critical portion or all of the rod is transformed to granules, figure 1d.



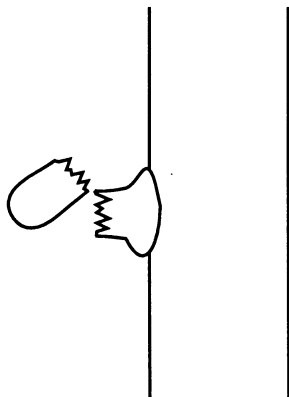
(a) Deflection

Fragment ricochets from an inclined armor surface



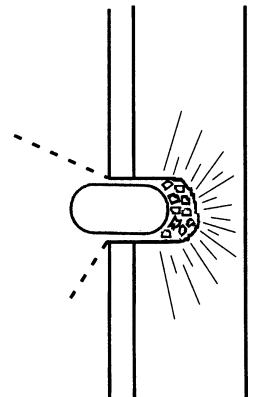
(b) Kinetic Energy Absorption

Fragment is slowed and stopped by plastically deforming armor



(c) Deformation and Fracture

Hard armor surface produces large stresses in fragment, blunting the leading edge and/or breaking it into two or more pieces



(d) Erosion

Confined ceramic erodes the leading edge of penetrating fragment and eventually reduces it to particles

CM-7412-17

FIGURE 1. PROJECTILE DEFEAT MECHANISMS

Depending on the size, shape, density and velocity of the fragment, and the characteristics of the target, a certain defeat mechanism may be more attractive than the others or a combination will be more effective. Contractors in the A/AA program made effective use of spaces in their armor designs. Spaces give projectile fragments the opportunity to rotate and disperse so that the load on target is not focused on a small area but instead is distributed over a larger area.

Minimum spaces (as when adjacent plates are simply butted up against each other) also have a degrading effect on a projectile. The failure process occurring in an initial armor plate must be reinitiated in a backing plate, and this is often energy consuming. For example, plugging failure of rolled homogeneous armor by a projectile often occurs by a shear instability, which requires considerable plastic flow to initiate and hence is difficult to propagate from one plate to another. Considerable thought has been given to the optimal interface bond strength in dual hard-steel armor.⁽⁸⁾

Similarly, angles can be used to advantage when designing for ballistic protection. The ability to cause projectile ricochet is an obvious benefit and should be exploited in design when feasible. Ricochet, however, typically requires a large angle and hence this defeat mechanism is often not space efficient. The angle can possibly be reduced somewhat by surface modifications that reduce friction, such as might be achieved by mechanically or chemically treating the surface.

Even in the absence of ricochet, inclined surfaces hold worthwhile threat degradation advantages. When a projectile must penetrate an inclined plate, the effective thickness of the plate is greater than the plate thickness by a factor of the cosine of the angle. Thus more material is put in the projectile path for the same barrier weight or alternatively the same amount of material can be presented at less weight.

An angled plate has a further advantage in that it imposes nonsymmetric lateral forces on a rodlike projectile and thus tends to deflect it from its original trajectory. Even a few degrees of yaw significantly decrease the penetrability of a projectile.

The inclined dual hardness armor is a design that attempts to invoke three mechanisms of projectile defeat. Dual hardness armors consist of a hardened outer steel backed by a softer steel. The outer layer produces large stresses in the projectile, tending to deform and fracture it; the backing layer flows plastically, absorbs kinetic energy, and tends to slow and stop the projectile; the inclined surface encourages deflection. Furthermore, when the armor surface is inclined to the threat direction, the threat encounters a greater effective thickness of armor.

A strategy used successfully by the Honeywell team⁽⁹⁾ in the A/AA program was to degrade the threat gradually as it penetrated the armor package. None of the armor elements in the package was capable by itself of defeating the projectile but by acting consecutively on a progressively degraded threat, the array of elements accomplished the defeat.

The success of the gradual-defeat strategy illustrated that, while no one material in any reasonable quantity had the properties to defeat these very formidable DOD threats, a combination of different types of materials (in this case metallic, ceramic, and polymeric materials) that invoke different projectile defeat mechanisms can be assembled in ways to achieve projectile defeat. This example also illustrates the effectiveness of spaces and angles in barrier design.

Similar strategies should be considered in designing barriers to defeat aircraft engine fragments. The strategies should be implemented by selecting materials having desirable properties (such as hardness, strength, toughness, plastic deformation capability, elastic elongation, and density) and configuring them to meet the ballistic requirements of the aircraft, within the weight, space, and cost constraints.

Several innovative armor elements were conceived or developed during the A/AA program and in other DOD armor programs. Steel plates containing cylindrical through holes and angled to the attack direction were found effective in defeating long-rod projectiles by breaking them into smaller pieces and dispersing them over an expanded area. When the holes were filled with glass, this armor demonstrated enhanced performance against shaped charge jets.

Urethanes, polysulfides, polyvinyl chlorides, and acrylics were successful in providing protection against damage (cracking or chipping) to ceramic tiles adjacent to tiles being attached. The elastomers with the highest tear resistance and adhesion performed best in their ability to contain fragments. Isodamp, a thermoplastic polyvinyl chloride produced by EAR, a subsidiary of CABOT Corporation, performed particularly well as a tile isolator and fragment retainer.

Felt batting made of unidirectional, high tenacity, continuous fiber yarn, made into bats and then needle-punched for added strength, is effective in absorbing energy from an impacting projectile. The mechanism involves the frictional losses as adjacent fibers slide over one another. Felts can be engineered to achieve highest ballistic performance at lowest density and cost by blending fibers of aramids, polyethylenes, PBO, and the like and, if desired, by needle punching to enhance the physical interlocking of crosslapped layers. Further strengthening is often attainable by thermobonding, i.e., applying pressure and heat so that one fiber melts and creates a unique bond throughout the textile. A drawback of felts is their tendency to absorb moisture and become heavy.

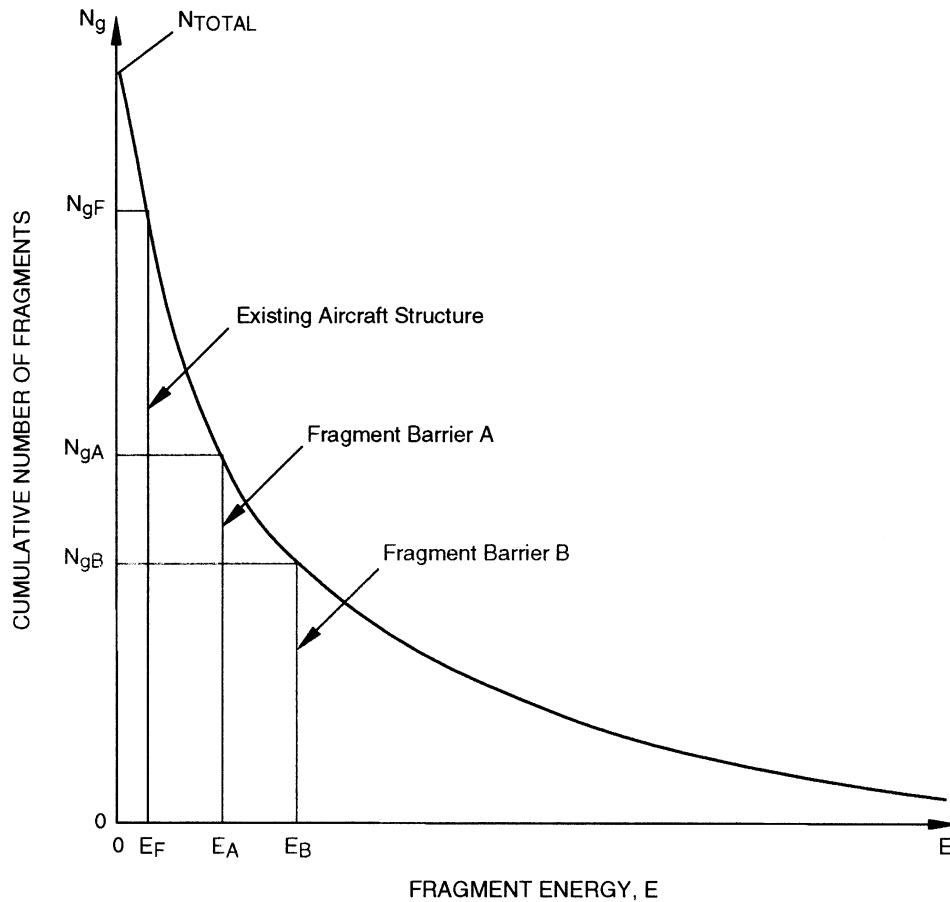
Several armor elements were developed that did not result in significant improvements in ballistic performance or in equal performance at less weight or cost. These included ceramic balls encapsulated in a polymer matrix, polymeric balls dispersed in a ceramic matrix, and a range of glasses both in monolithic and multilaminate geometries.

THE ENGINE FRAGMENT THREAT

CHARACTERISTICS OF AIRCRAFT ENGINE FRAGMENTS.

Under a separate Interagency Agreement from the FAA, the Navy Air Warfare Center (NAWC) is collecting and analyzing data from previous engine failures to define the fragment threat.⁽³²⁾ When the NAWC findings on turbine engine fragment characteristics become available, this information can be used to more precisely specify requirements for barrier designs. Until then, the fragment energy and trajectory definitions given by the Federal Aviation Regulation, (FAR) AC 20-128 and Joint Airworthiness Regulation, (JAR) Part 25.901 regulation can be used. These regulations define three categories of fragments: (1) bladed 1/3 disk, (2) 3-blade rim sector, and (3) small fragments.

Initially, we are considering two classes of engines: large engines for commercial transport and small commuter engines and Auxiliary Power Units (APUs). We assume that an engine failure releases a population of small fragments that has a more or less continuous distribution of energies such as indicated in figure 2. The fuselage structure will stop very small, low-velocity fragments having energies less than E_F . We envision designing barriers that truncate this distribution at higher fragment energies such as E_A and E_B . Such barriers will neutralize larger and faster fragments but will weigh and cost more. The relationship between fragment mitigation benefit and economics should be defined to assist decisions regarding barrier design.



CM-7412-5A

FIGURE 2. HYPOTHESIZED FRAGMENT ENERGY DISTRIBUTION SHOWING HOW BARRIERS OF INCREASING ENERGY ABSORPTION CAPABILITY TRUNCATE AN INCREASING NUMBER OF FRAGMENTS

The fragments emanating from a failed turbine engine range downward in mass from many kilograms for one-third turbine disks to a few grams for bits of cowling and fan blades. The fragment mass distribution will vary with engine type and accident scenario. The most available clues to fragment characteristics are the holes produced in the aircraft structure by the fragments and the fragments themselves. Unfortunately, no a priori method exists for deducing from hole size characteristics the size, shape, velocity, or energy of the fragments. However, accident investigators have painstakingly recovered fragments produced in accidents and sought to correlate fragment characteristics with the damage produced. From such correlations and from a knowledge of engine components and their velocities, useful estimates of fragment characteristics can often be made.

Tilzey⁽³³⁾ reviewed the historical records related to uncontained engine failures in aircraft (49 events) over the past 25 years and analyzed the hole sizes in the aircraft structures. He found that over 80% of the holes had maximum dimensions of 3 inches or less, and that nearly 90% of the holes had maximum dimensions of 5 inches or less. In several of the accidents, it was the

relatively small fragments that caused the critical aircraft damage. These findings lead us to focus on small fragments in our efforts to develop barriers for mitigating catastrophic effects of uncontained engine debris on aircraft.

Because a method does not currently exist to infer fragment size from the size of the hole it made in the fuselage, we arbitrarily chose fragment masses of 25 and 95 grams as the masses to be defeated in this study. The fragment data survey being conducted at the NAWC is expected to provide further information that can be used to evaluate this choice.⁽³²⁾

Similarly, the shapes of the fragments are varied and largely unknown. In hopes of generating data that could be compared directly with data from previous studies, we reviewed the literature and contacted the technical community to determine if a consensus fragment simulator existed.

Finding that a consensus fragment simulator did not exist, we again arbitrarily selected a rectangular plate with truncated corners (as discussed later). This shape incorporates the important features of many turbine engine fragments that we have examined. The truncated corners on the impacting surface are reminiscent of those on the cylindrical fragment simulators used by the military. A Boeing study⁽³⁴⁾ used such a cylindrical geometry to examine the ballistic performance of certain aircraft structures. Because many uncontained fragments are from engine parts made from titanium alloys, we elected to machine the fragment simulators from Ti-6Al-4V.

Airframe and engine manufacturers estimated that fragment velocities range from 200 to 700 ft/s (60 to 210 m/s) after the fragments have left the nacelle space. The above considerations for fragment size, shape, and velocity formed the bases for the impact experiments to evaluate barrier performance described in a later section of this report.

CRITICAL FRAGMENT-VULNERABLE AREAS ON AN AIRCRAFT.

Discussions with airframe and engine manufacturers suggested four systems that are critical for continued safe operation and landing of an aircraft: the flight control lines, the fuel lines, the engines, and the pressure boundary. The flight control lines, which are separated spatially in the aircraft and are redundant, must not be severed by engine fragments. Likewise, second or third engines need to be operational and thus must not be incapacitated by fragments from a failed engine. Finally, compromise of the pressure boundary (holes and tears in the fuselage wall, for example) at typical cruising altitudes could be catastrophic. We address each of these systems in turn.

Fuel lines and flight control lines, whether hydraulic, wire, or optical, are likely to be most efficiently protected by local barriers positioned near the line and in the path of the expected fragment trajectory. Such barriers would make use of existing aircraft structure such as longerons, cargo bay floor, and baggage.

Second and third engines can be protected by barriers placed inside the nacelle over an area that subtends the solid angle defined by possible fragment trajectories. The area to be protected may also be adjusted to include fragments that ricochet from the runway should engine failure occur during taxiing. Barriers in the nacelle may also enhance fragment containment in the failed engine. Elevated temperatures may be a consideration in designing structures inside the engine nacelle.

Engines can also be protected by incorporating barriers in the space within the fuselage wall, i.e., the 4- to 5-inch distance between the outer aluminum fuselage skin and the interior trim (refer to the ValuJet incident of June 1995 in which a fragment from one engine penetrated the near and far fuselage walls and struck the nacelle of the engine mounted on the far fuselage wall⁽³⁸⁾). Such barriers will also enhance protection of control lines.

Barriers to conserve the pressure boundary will need to minimize areas of perforation and prevent widespread tearing of the fuselage skin.

Although mitigating the catastrophic potential of engine fragments requires that critical systems such as these be protected, accomplishing mitigation at minimum cost and minimum added weight requires that noncritical areas be left unprotected. Gunderson⁽³⁵⁾ identified the critical areas based on engine and airframe geometry. Tilzey⁽³³⁾ analyzed holes in aircraft from uncontained engine failures and thus provided experience-based information on the areas of an aircraft likely to be impacted by fragments. By combining both types of analyses, we can estimate the areas to be protected and the level of protection required in various areas.

FRAGMENT BARRIER DESIGN

We combined our findings to conceptualize fragment barriers for commercial aircraft after having reviewed the military armor literature and evaluated armor materials in terms of ballistic performance, density, and cost; having specified the characteristics of a representative aircraft engine fragment; and having identified critical fragment-vulnerable areas on an aircraft. It is clear that weight efficient and cost-effective barrier systems must be constructed from a combination of materials and must make judicious use of geometrical configuration, spaces, and angles. Furthermore, specific structures must be designed for specific critical aircraft systems, because a structure well suited for protecting a control line, for example, may not be well suited for protecting the second engine.

The challenge was to devise a strategy to slow, stop, or divert a fragment of given characteristics (mass, velocity, geometry) and to design a barrier structure that implements this strategy and has minimum weight and cost. Such a challenge was successfully met in devising armor systems to protect main battle tanks from very high-energy weapons. Winning strategies were those that gradually and progressively attacked the threat until the threat was defeated. We adopted similar strategies here.

FUSELAGE WALL FORTIFICATION.

In recent years, catastrophic and near catastrophic incidents were caused by engine fragments that penetrated the fuselage wall and damaged control lines (1989),⁽³⁶⁾ fuel lines (1993),⁽³⁷⁾ and the second engine (1995).⁽³⁸⁾ To reduce the likelihood of such incidents, we considered a barrier system that is implemented within the fuselage wall.

Depending on aircraft type, up to 4 to 5 inches of space exist between the outer fuselage skin and the interior trim of the cabin. The circumferential frame and longitudinal stringers create a grid of thicker, more fragment-resistant aluminum structural beams encompassing roughly 9- by 20-inch areas, figure 3. Within this grid, only the 0.036-inch aluminum skin, the fiberglass insulation blanket, and the 0.100-inch interior trim are in the path of an engine fragment,

figure 4a. These areas offer little resistance to penetration from fragments and any critical component behind would be impacted with nearly the entire energy of the fragment. We sought barriers to slow or stop fragments that strike areas within the grid boundaries.

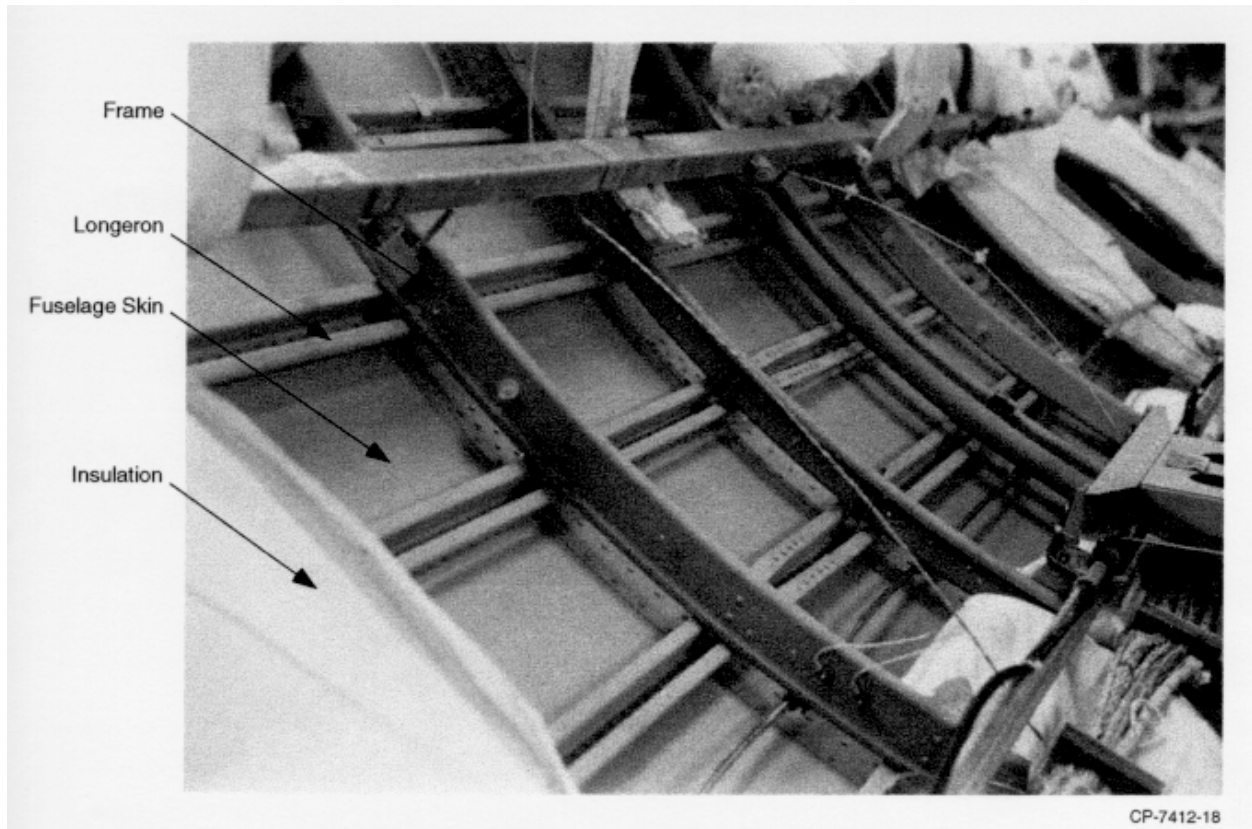
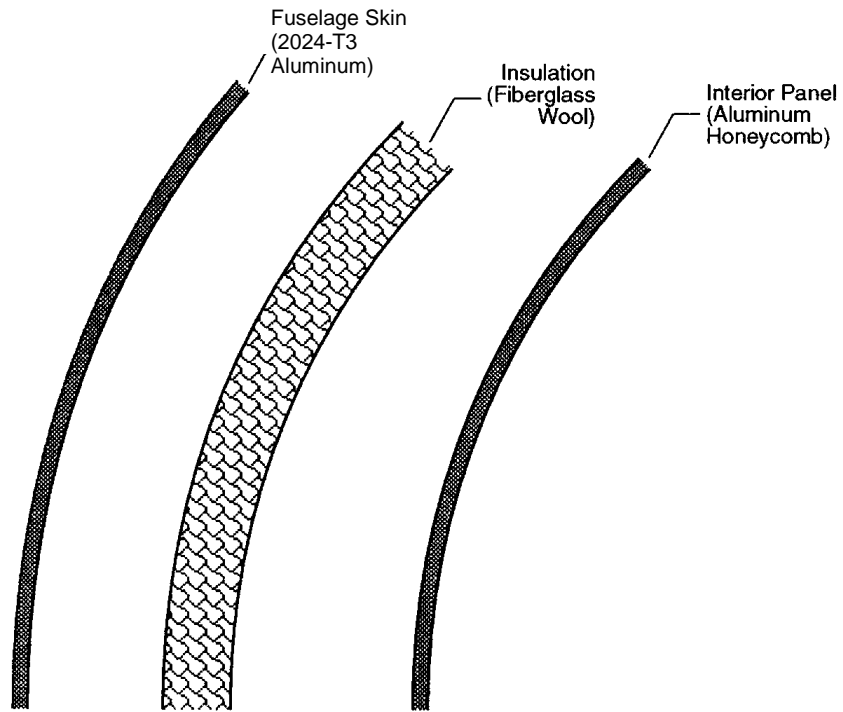


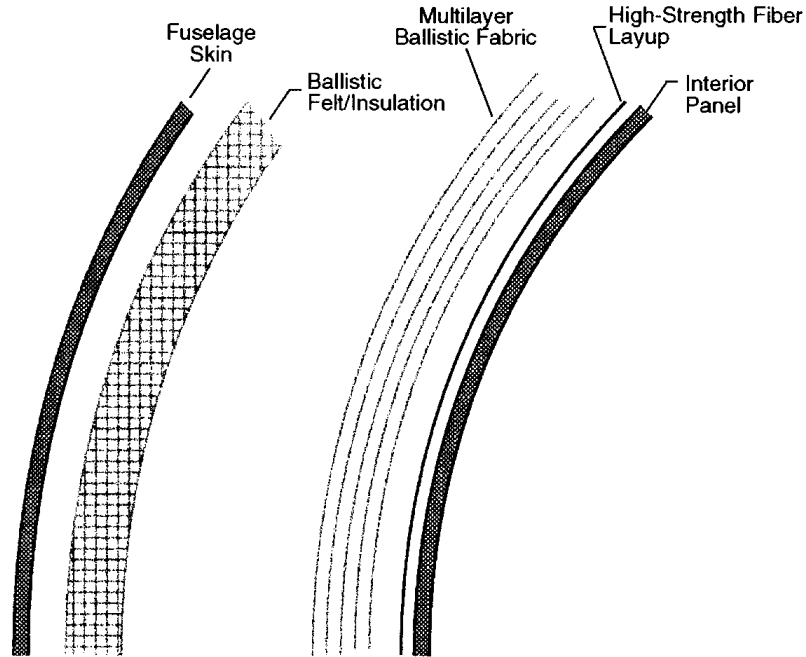
FIGURE 3. FUSELAGE WALL WITH INTERIOR PANEL AND INSULATION REMOVED TO REVEAL STRUCTURE

To minimize the added weight, we chose to use low-density materials having high specific ballistic protection that can simultaneously perform the functions of, and perhaps replace, existing materials. The existing materials in the fuselage wall are the fiberglass blanket and the interior paneling. Their replacement with ballistic materials thus requires the ballistic material to provide adequate thermal insulation, acoustic insulation, flame resistance, moisture resistance, and aesthetics. From the standpoint of fire, three issues are critical: flammability, smoke production, and toxicity of the gas produced. With these objectives in mind, we designed the barrier system using high-strength polymer fibers in the form of felt, weaves, and 0°, 90° resin-bonded layups.

We envisioned a barrier consisting of a layer of ballistic felt positioned near the fuselage skin, a multilayer of resin-bonded fiber layup attached to the inner surface of the paneling wall, and, as needed to stop fragments of chosen higher energy, a multilayer of woven high-strength polymer in between, figure 4b.



(a) Cross section of fuselage wall.



(b) Cross section of fuselage wall with fragment protection

CAM-7412-13A

FIGURE 4. TYPICAL FUSELAGE WALL AND BALLISTICALLY REINFORCED FUSELAGE WALL

The ballistic felt is held by attachments at the frame and longerons close to the outer fuselage skin but stands off a small distance so as not to trap moisture against the skin and cause corrosion. The felt has two ballistic functions: to slow the fragment and blanket the sharp edges of the fragment tip. As the felt engages the fragment and is torn from its lateral fasteners, it deforms substantially, absorbs some energy, and slows the fragment. More important, it does not get penetrated and rides with the fragment to present a larger area and a blunter leading edge to the next barrier layer. It may also impart some rotation to the fragment.

The next part of the barrier is a multilayer of strong fibers, most likely in a 0°-90° bonded layup affixed to the interior side of the interior paneling. The number of layers will depend on the size and velocity of the fragment chosen to protect against. The material may be polyethylene (such as Spectra Shield) which has the advantage of low density but is not particularly flame resistant, or aramid (such as Gold Shield) which is decidedly more flame resistant but 50% more dense. Both materials have excellent strength and ballistic properties. An emerging material is PBO, which is stronger than either aramid or polyethylene, has high flame resistance, and has density comparable to aramid but (at the moment, at least) is more expensive than either and not available in large quantities. A combination of two or all of these materials may provide the optimal solution.

Another consideration in choosing barrier materials is moisture absorption. Polyethylene and PBO fibers absorb up to 2% of their weight, whereas other fibers such as nylon and aramids absorb 5% or more. Moreover, because of their open structure, felts made from these materials tend to absorb and retain additional moisture. To inhibit moisture retention, the felt could be encapsulated with the moisture bag material currently used for the fiberglass insulation. Or to obtain an additional increment of ballistic resistance, the encapsulation bag could be one or more layers of a strong, impervious-to-water material such as a bonded fiber layup (Spectra Shield or Gold Shield, for example). This configuration may allow the felt to replace the current insulation and provide cost- and weight-effective additional ballistic protection.

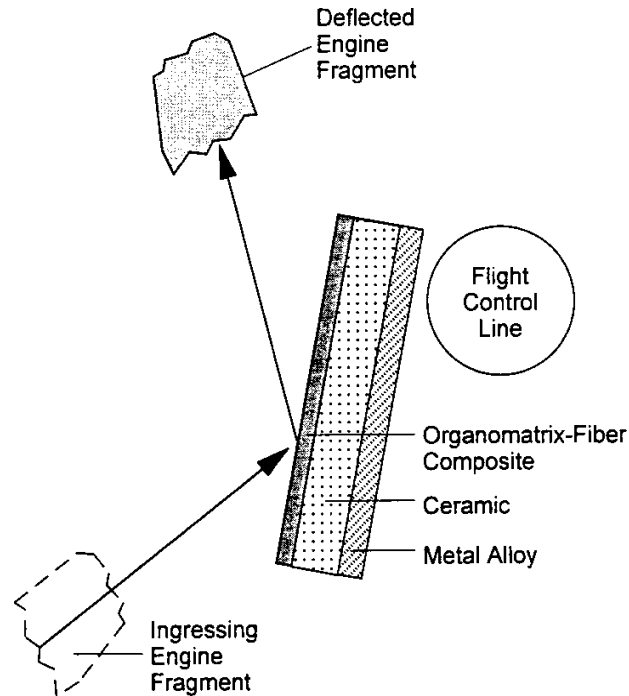
If it is desired to protect against higher-energy fragments, the number of layers in the layup can be increased or a multilayer woven of a high-strength polymer fiber could be added between the felt and the paneling. The degree of protection afforded by any of the designs will need to be determined with fragment impact experiments. A key parameter governing the amount of energy absorbed by the felt and the multilayer layup is the strength with which they are fastened to the frame and longerons. To exploit the ballistic properties of the layup fully, the fastening strength must be greater than the fiber strength. Conversely, the fastening strength for the felt should ideally be slightly less than the penetrating strength to allow the felt to blunt the fragment as it impacts the multilayer. The ballistic resistance of any barrier system attached to the fuselage skeleton is limited by the strength of the fuselage skeleton. If the barrier layers are attached to the skeleton and are not penetrated by the fragment, the barrier will load the skeleton until the fragment is stopped or until the skeleton deforms and buckles. Thus preventing penetration of a large, energetic fragment may result in indentation of a sizable area of the fuselage. Although such an indentation may cause trauma to passengers in the vicinity, it would most probably not result in catastrophic loss of the aircraft.

The choice of material and the details of the design should be established systematically in a research program that evaluates parametrically the many combinations of likely variations using

experiments and computations. Designs should be sought that provide the optimal combination of ballistic protection, added weight, and cost.

LOCAL PROTECTION OF CONTROL LINES AND FUEL LINES.

Control lines and fuel lines might be protected from a fragment that penetrates the fuselage by a barrier located close to the line consisting of a plate of ceramic wrapped in strong polymer fibers and backed with an aluminum plate. The barrier effectiveness would be enhanced by tilting the barrier surface to the expected fragment trajectory to encourage ricochet, figure 5.



CM-7412-7A

FIGURE 5. FRAGMENT BARRIER FOR FLIGHT CONTROL LINE PROTECTION

This design is inspired by the DOD advanced armor program which showed that ceramics provided significant ballistic advantage and at lower total weight than steel armor. Since ceramics are much harder than engine materials, they will tend to deflect, deform, and fracture impinging engine fragments. To be most effective, however, the ceramic needed to be encased, usually in steel or fiber-reinforced resin, to keep the shattered ceramic material in the path of the penetrator and to provide multihit protection. For application in aircraft, encasement with low-density polymer fibers should be considered. Furthermore, a backing plate of tough material often enhanced performance. Perhaps a strip of steel, titanium, or aluminum would give equal resistance at lower cost, although at greater weight. Such tradeoffs need to be examined.

FRAGMENT BARRIERS WITHIN THE NACELLE.

Another suitable barrier location for uncontained engine fragments on commercial aircraft is immediately outside the engine containment ring but within the nacelle. Locations close to the

hot sections of the engine will require barrier materials that are more resistant to elevated temperature. As required for barriers in the fuselage wall and close to control and fuel lines, all barriers must be lightweight, space-efficient, and inexpensive. If possible, they should also serve one or more other functions in addition to ballistic protection such as noise suppression (incorporation of elastomers, spaces, styrofoam, and the like) structural stability, firewall, and insulation.

CONTAINMENT.

Although this study was aimed specifically at uncontainment, i.e., the protection of critical aircraft components from engine debris not contained in the engine (FAR 25), the survey of advanced military armor materials, barrier concepts, and configurations produced information that promises to also be useful in containment, as described in FAR 33.

Containment barriers are of two types: those in the immediate vicinity of the hot section that must withstand high temperatures and those somewhat removed from the hot section that have only moderate or no temperature resistance requirement. For the former, ceramics, nickel-based alloys, some cermets, and titanium alloys are suitable materials. As is the goal for uncontainment, the key for containment is to configure some combination of these materials that provide the desired ballistic protection at acceptable weight, space, and cost.

Currently, containment rings are made from high-density alloys. Significant weight savings could be realized if equivalent containment could be achieved with ceramic. Lane⁽³⁹⁾ concluded that a fan blade containment system consisting of ceramics (Al_2O_3 , SiC, and B_4C) is more weight-efficient than metals (steel, Ti, and Al) or fiberglass and polymer fibers. A ceramic containment ring is likely to perform better if it is encased in a tougher material to prevent dispersion of fragments. For very hot areas of the engine, encasement of the ceramic with nickel-based alloy may be required but at engine locations where lower temperatures prevail containment could be accomplished at less weight with titanium. At still cooler areas, strong polymer fibers may be the encasement material of choice.

High-strength polymers show promise for containment around low-temperature sections of engines. DeLuca and Petrie⁽⁴⁰⁾ performed spin-pit tests on fiberglass/polyester, fiberglass/phenolic, Kevlar/phenolic, fiberglass/polyester-steel, fiberglass/phenolic-steel, Kevlar/phenolic-Ti, and Ti and found that all successfully contained the high-energy fragments from a burst T53 turbine motor. Pepin⁽⁴¹⁾ demonstrated the effectiveness of a three-dimensionally reinforced containment ring made from PBO and other high-strength polymer fibers.

As has been postulated for the uncontainment problem, efficient containment may be best accomplished by the gradual defeat strategy. Using the space between the blade tips of the turbine engine and the outer skin of the nacelle, the kinetic energies of blades and discs can be progressively reduced as the fragments interact with barrier layers in their path. To achieve containment with minimum additional weight and cost requires choosing the most appropriate materials and configuring them in the way that takes best advantage of their fragment-resistant properties.

The Boeing Company evaluated the effect of the existing engine structure on the progressive degradation of fragment energy.⁽⁴²⁾ Testing performed on a thrust reverser structure validated a

numerical model of impact resistance and showed that the cowling, cascades, and blocker doors reduced the energy of engine debris by more than 50%. The authors concluded that the uncontained fragments were reduced enough in size and weight to be manageable with minimal shielding in the fuselage wall.

Stotler⁽⁴³⁾ found that a layer of Kevlar felt was not effective in enhancing containment of turbine blades in blade-out tests of the General Electric TF34 engine. Stotler's thought was to enmesh the released blade in the very light, bulky, and tough felt thus increasing the apparent area of the blade as it attempted to penetrate through the eight plies of Kevlar cloth wrapped around the steel containment structure. The experiment showed that, although the felt wrapped around the sharp edges of the root section of the blade and restricted its ability to penetrate the Kevlar cloth, the cloaked blade pulled the Kevlar cloth further in the impact direction and resulted in greater overall damage. Much of the blade system was outside the containment system and a considerable portion of the containment ring was left unprotected from any later impact. However, for the uncontainment problem, multihit capability is not as large a concern because uncontained fragments are typically dispersed in space.

FRAGMENT BARRIER EVALUATION

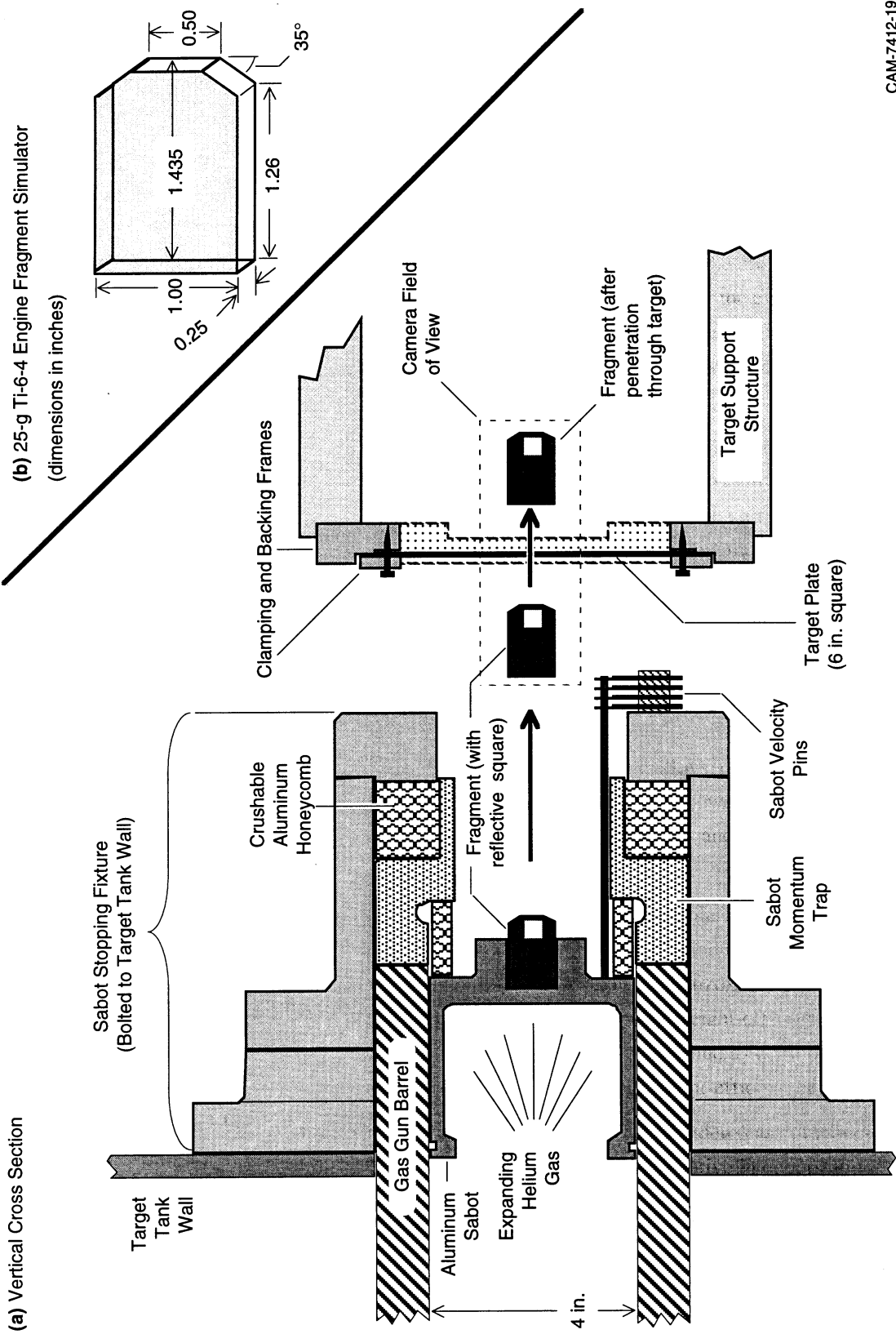
IMPACT EXPERIMENTS.

The SRI gas gun facility was used to perform experiments to evaluate the impact response of barrier materials and systems. The 4-inch-diameter bore, 48-foot-long gas gun was modified to allow acceleration of fragments or fragment simulators having a maximum transverse dimension of 1.75 inches to velocities ranging to 700 ft/s. Fixturing was designed and built to hold targets 6 or 12 inches square at any orientation from 0° to 65° to the fragment trajectory. Figure 6(a) is a schematic of the fragment impact facility.

The fragment simulator, shown in figure 6(b), is mounted on the front of an aluminum sabot which is accelerated down the evacuated barrel of the gun. The sabot is slowed and then stopped by a momentum trap and by rings of crushable aluminum honeycomb located at the end of the barrel, while the fragment simulator continues to travel toward the target. Achieved velocities are within 3% of prescribed. The targets are clamped tightly around their peripheries, as shown in figure 7(a), leaving a free region of 5.25 inches square for the 6-inch target configuration.

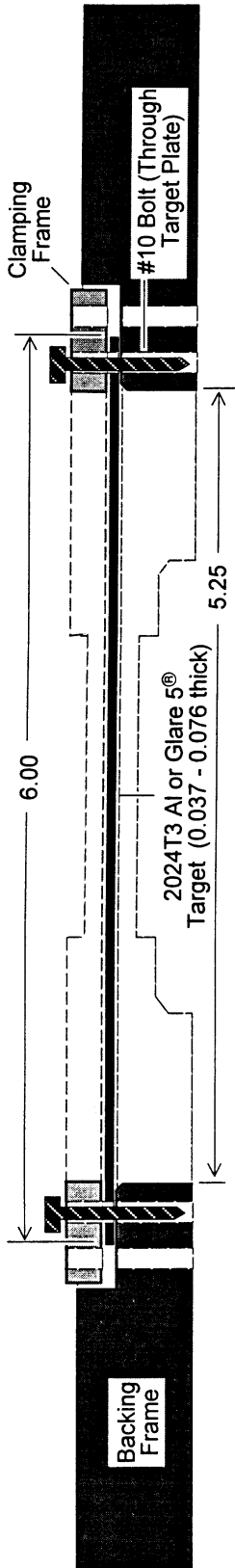
A high-speed camera with framing rates of about 20,000 frames per second is focused on the regions in front of and in back of the target to record both the initial velocity and orientation of the fragment before impact as well as the residual velocity and orientation of the fragment after target penetration or ricochet. A square of highly reflective tape is attached to the side of the fragment simulator to enhance its visibility. An independent measurement of the velocity of the sabot before reaching the stopping fixture is provided by contact pins positioned in the barrel at the muzzle; these pins also trigger the light sources for the high-speed photography.

Tests were performed in which the fragment simulators impacted the barrier systems with the end having the truncated corners (as indicated in figure 6). Because the penetrability of a fragment of given mass and velocity depends on its orientation at impact (sharp-edged fragments penetrate more easily than blunt-edged fragments), impact tests were performed with both blunt and corner orientations of the fragment.

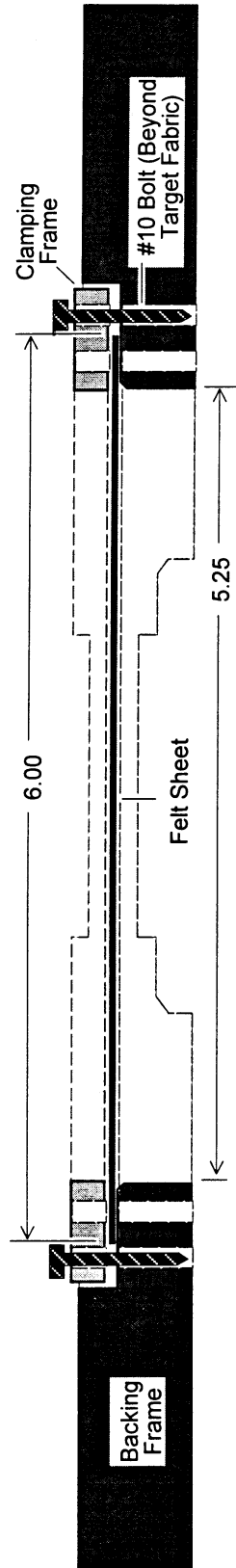


CAM-7412-19

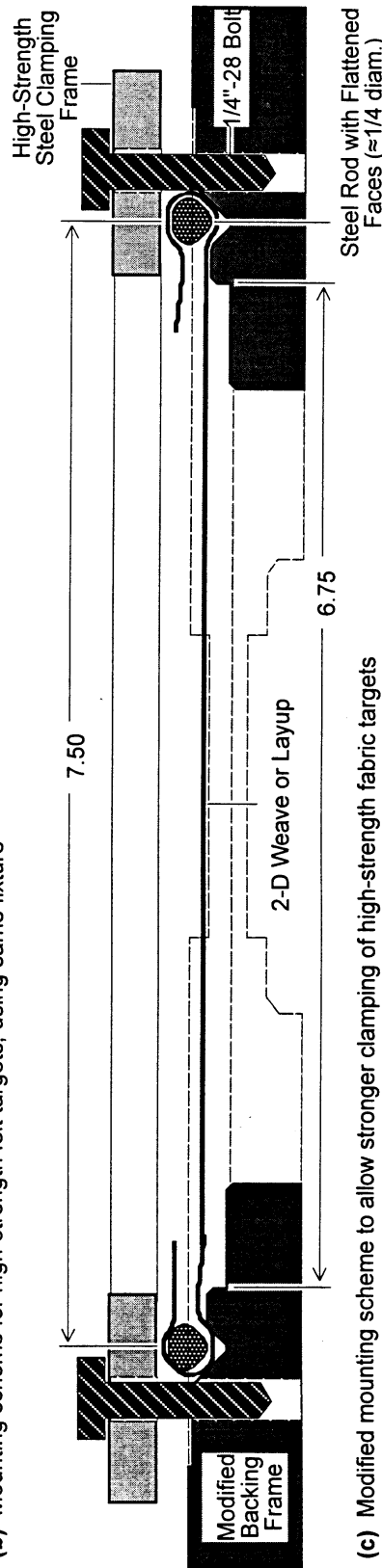
FIGURE 6. SRI GAS GUN FACILITY FOR EVALUATING POTENTIAL ENGINE FRAGMENT BARRIERS (6-in.-SQUARE TARGET, 0° TILT CONFIGURATION SHOWN).



(a) Mounting scheme for rigid plate targets



(b) Mounting scheme for high-strength felt targets, using same fixture



(c) Modified mounting scheme to allow stronger clamping of high-strength fabric targets

CAM-7412-20

FIGURE 7. VARIOUS TARGET MOUNTING AND CLAMPING SCHEMES USED IN GAS GUN IMPACT TESTS TO EVALUATE POTENTIAL ENGINE FRAGMENT BARRIERS. ALL DIMENSIONS IN INCHES

Experiments were first performed to measure the inherent ballistic resistance of the fuselage skin and glass-reinforced aluminum. Initial experiments were conducted with 25-gram Ti-6Al-4V fragment simulators and 6-inch-square sheets of 0.040-inch-thick 2024-T3 aluminum (typical of fuselage skin) and 0.036-inch-thick Glare 5[®], a commercially available fiber-metal laminate consisting of cross-plyed glass fibers in epoxy between two layers of 2024-T3 aluminum*. The energy absorbed was measured and compared. Impacted targets were examined to determine details of the penetration mechanisms.

Table 5 presents the relevant experimental parameters and results, including the velocities and orientation of the impactor before and after impact and the kinetic energy lost. The 12 tests included two thicknesses of 2024-T3 Al fuselage skin material—1.02 mm (0.040 in.) and 1.58 mm (0.062 in.)—and two thicknesses of Glare 5[®]—0.94 mm (0.037 in.) and 1.93 mm (0.076 in.). The tests spanned a range of impactor velocity from 37 to 127 m/s (121 to 417 f/s) and resulted in a range of impactor orientation from 0° to 22° in pitch at impact. Half of the tests resulted in complete penetration, while half resulted in target deformation or partial perforation and eventual impactor rebound.

Figure 8(a) shows three representative frames from Test 8 in which the impactor fully penetrated a 1.02-mm-thick (0.040 in.) aluminum target at a velocity of 81 m/s. The impactor is shown at three stages of flight: before impact, during penetration, and after full penetration. Figure 8(b) shows three frames from Test 7 in which the impactor partially perforated a 0.94-mm-thick (0.037 in.) Glare 5[®] plate and then rebounded. The impactor is shown before impact, at the point of maximum plate deformation, and during rebound (it actually makes a 180° turn around the vertical axis; the rebound picture shows the side that does not have the reflective strip).

Figure 9 shows photographs of the aluminum and Glare 5[®] targets from Tests 7 and 8. The phenomenology of penetration is as follows. The target deforms in a diaphragm bending mode, first elastically and then plastically. Transient deflections as large as 11 mm (0.43 in.) and permanent deflections as large as 5 mm (0.20 in.) are observed at the center of aluminum targets that experience no perforation damage. For high enough impact velocities, (Mode II) shear cracks originate at the front surface of the target at the location of the impactor edges and propagate through the target. Because of the shape of the impactor and its orientation with respect to the target at impact, the shear cracks from the target edges will originate and propagate at different times.

When the first shear crack reaches the rear surface of the target, partial perforation begins (see figure 9(d)). When cracks on three of the indentation sides have reached the back surface, and if the impactor is still traveling at a sufficient velocity, the partially perforated section of the target in front of the impactor will bend backward, hinging toward the side of the remaining ligament. This bending inhibits the propagation of the shear cracks within that ligament but promotes the extension of the fracture at either end of the ligament by Mode III shear cracking. After sufficient bending of the partially perforated section, the impactor can complete its penetration of the target (see figure 9(b)).

* Structural Laminates Company, 510 Constitution Blvd., New Kensington, PA 15068-1327.

TABLE 5. GAS GUN IMPACT TESTS USING AIRCRAFT SKINLIKE MATERIALS

Test No.	Target		Areal Density (g/cm ²)	Impactor (Before Impact)			Impact Results	Impactor (After Impact)				
	Material	Thickness (in.)		Velocity (m/s)	K.E. (J)	Pitch ¹ (°)		Roll ² (°)	Velocity ³ (m/s)	Pitch ¹ (°)	K.E. (J)	K.E. Lost (%)
1	2024-T3 Al	0.040	0.27	37	17	-10.1	-5.5	-13.8	-2.9	2.4	14.8	86
2	2024-T3 Al	0.040	0.27	42	22	+1.4	-8.5	-15.3	-3.0	3.0	19.2	86.7
3	2024-T3 Al	0.040	0.27	49	30	-13.3	-10.0	-6.8	+0.7	0.6	29.4	98
4	Glare 5 [®]	0.037	0.22	59	44	+17.1	+2.4	-8.4	-3.1	0.9	42.9	98
5	2024-T3 Al	0.040	0.27	56	39	+22.0	-29.7	-9.5	-18.1	1.1	38.3	97.2
6	2024-T3 Al	0.040	0.27	95	112	-9.3	-9.5	+61.8	-9.5	48.0	64.3	57.2
7	Glare 5 [®]	0.037	0.22	82	85	+2.2	+10.3	-3.9	+11.0	0.2	84.4	99.8
8	2024-T3 Al	0.040	0.27	81	83	+12.0	+2.0	+50.7	+11.5	32.3	50.2	60.8
9	Glare 5 [®]	0.037	0.22	92	106	+20.3	N.A.	+59.7	+34.6	44.8	61.6	57.9
10	Glare 5 [®]	0.037	0.22	80	80	+0.0	+1.2	+15.2	-14.9	2.9	77.0	96.4
11	2024-T3 Al	0.062	0.43	93	109	+14.0	+2.5	+4.6	+4.7	0.3	108.5	99.8
12	Glare 5 [®]	0.076	0.45	127	203	+0.0	-17.3	+75.8	+3.8	72.3	130.6	64.4

¹As observed by camera in horizontal plane ("+" = nose down, "-" = nose up). For nonzero roll, it is a combination of pitch and yaw.

²As determined from deformation of target ("+" = clockwise from vertical, "-" = counter-clockwise from vertical).

³Positive velocities denote residual velocity after penetration; negative velocities denote velocity after rebound.

Test 8: Aluminum Fuselage Skin

81 m/s into 0.040-in.-thick 2024-T3 Al
(Full Penetration)

Test 7: Glare 5®

82 m/s into 0.037-in.-thick Fiber-Metal Laminate
(Partial Perforation and Rebound)

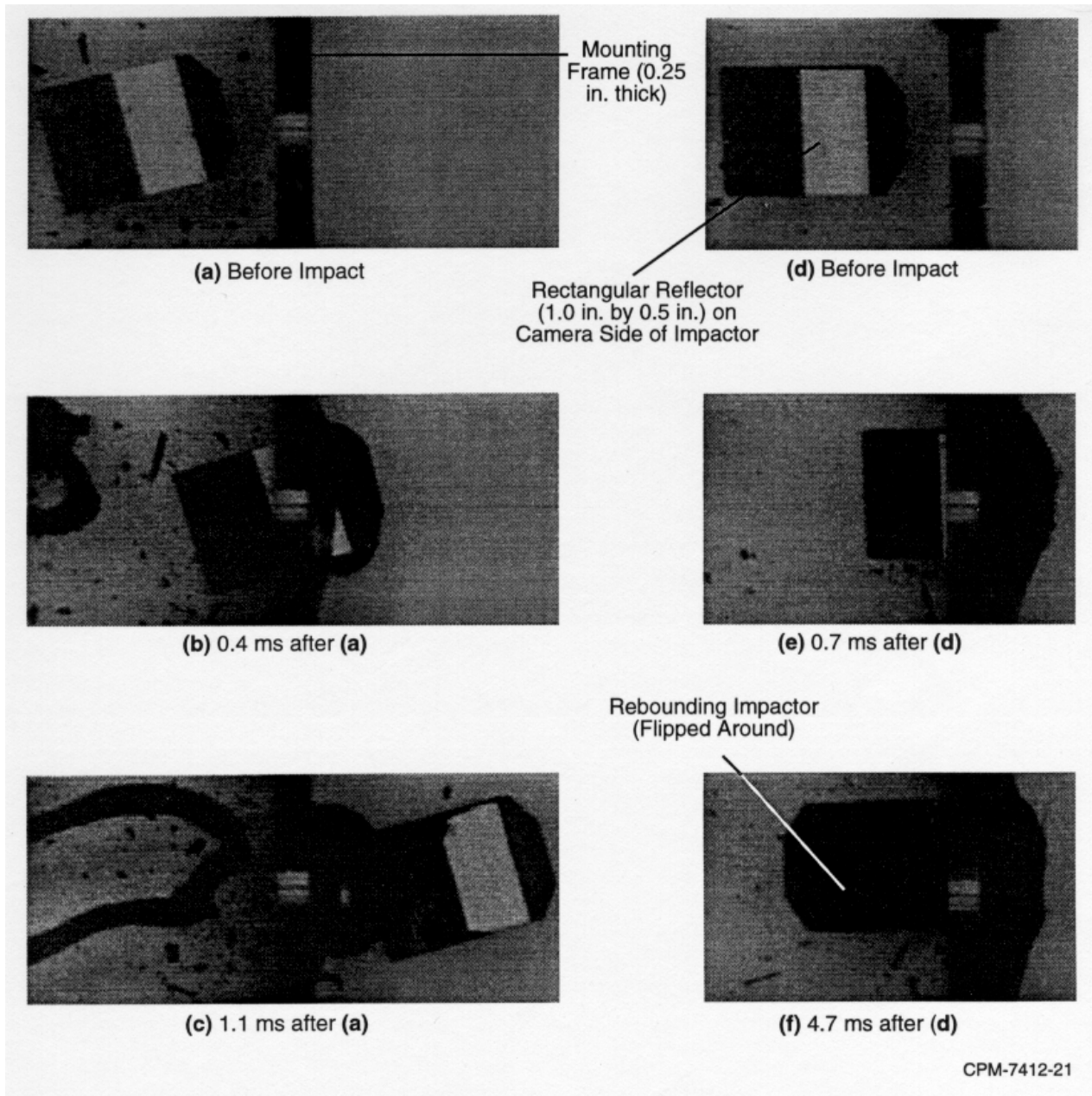
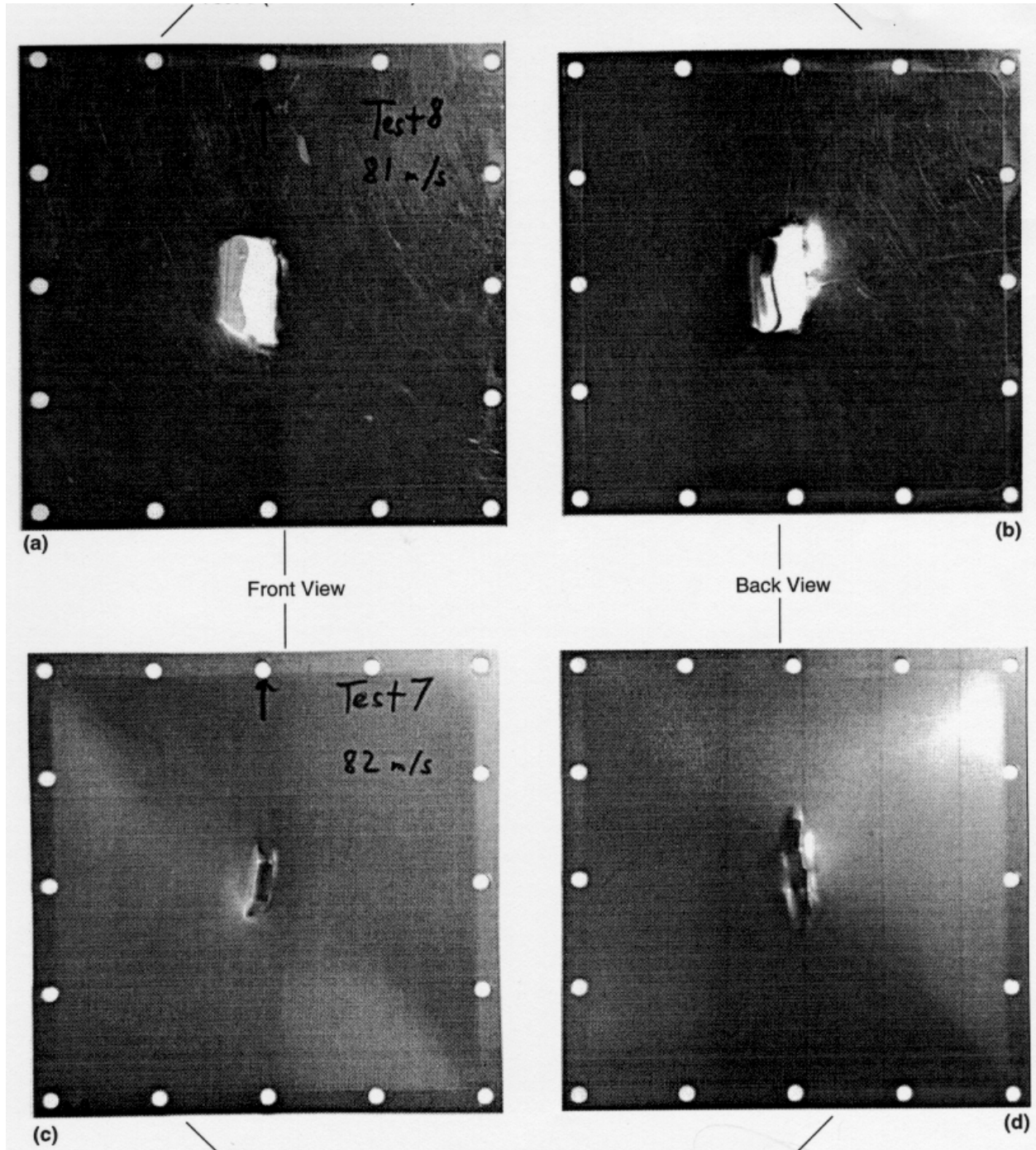


FIGURE 8. REPRESENTATIVE FRAMES FROM HIGH-SPEED CAMERA FOR TWO FRAGMENT IMPACT TESTS

Test 8 Aircraft Fuselage Skin —81 m/s into 0.040-in.-thick 2024-T3 Aluminum



Test 7 Glare 5[®]—82 m/s into 0.037-in.-thick Fiber-Metal Laminate

FIGURE 9. RECOVERED 6-in.-SQUARE TARGET PLATES FROM TWO FRAGMENT IMPACT TESTS

Figure 10 plots the energy absorbed by the target during the interaction with the impactor versus the target's areal density. Straight lines were drawn between the data points representing energy absorbed during full penetration for the two types of material. The result appears to be that a 6-in.-square Glare 5[®] target can absorb considerably more energy in slowing the impactor than a 6-in.-square 2024-T3 Al target of the same areal density. Differences in the orientation of the impactor at impact (i.e., pitch) may account for some of the variability in the results.

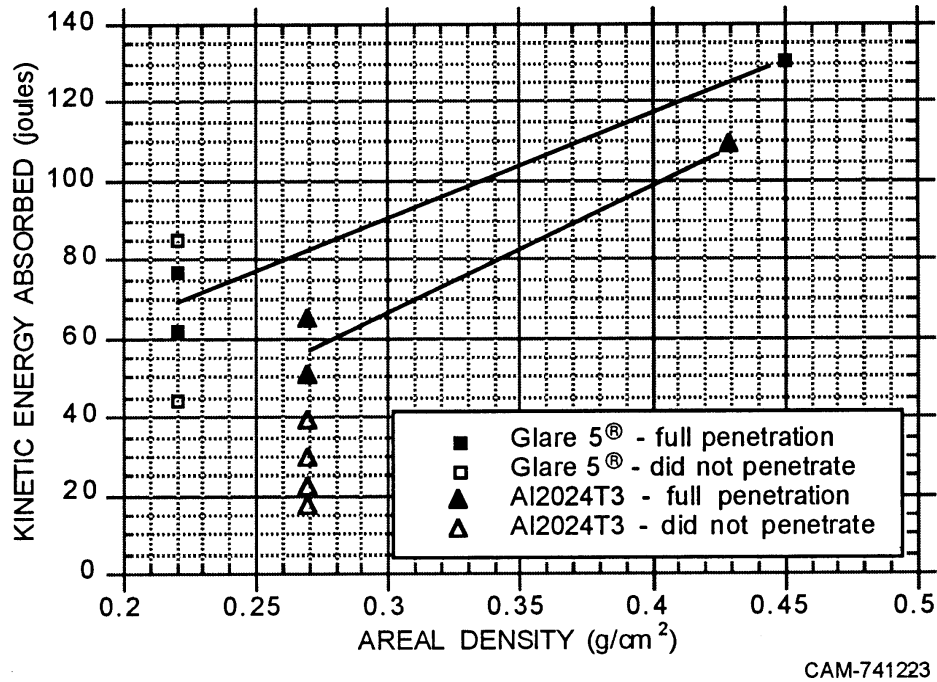


FIGURE 10. KINETIC ENERGY ABSORBED BY 6-in.-SQUARE TARGETS DURING IMPACT BY 25-GRAM FRAGMENT SIMULATOR AT 80 m/s

HIGH-STRENGTH FABRIC MATERIALS.

For the next series of tests, various fabric materials were investigated that might be placed in the space between the outer fuselage skin and the interior trim. These materials were made of high-strength fibers in the form of layups (with 0° and 90° plies), felts, and two-dimensional weaves. Table 6 lists the various materials we were able to obtain, along with some relevant parameters. These materials are described later.

TABLE 6. HIGH-STRENGTH FABRIC MATERIALS OBTAINED FOR IMPACT STUDIES

Trade Name	Supplying Company ¹	Fiber Material	Fabric Type	Approximate Thickness		Areal Density (g/cm ²)
				(in.)	(mm)	
Spectra Shield	Spectra Performance Materials	Aramid	Layup (0° and 90° plies)	0.009	0.23	0.0255
Gold Shield	Spectra Performance Materials	UHMW polyethylene ²	Layup (0° and 90° plies)	0.006	0.15	0.0136
Zylon	Toyobo Co., Ltd.	PBO	2-D weave	0.010	0.25	0.0219
TurtleSkin	Warwick Mills	Aramid	2-D weave	0.011	0.27	0.0241
—	Spectra Performance Materials	UHMW polyethylene	Felt	0.13	3.3	0.0309
—	Spectra Performance Materials	Aramid	Felt	0.09	2.3	0.0115

¹Spectra Performance Materials is located in Petersburg, VA; Toyobo Co., Ltd., is in Osaka, Japan; Warwick Mills is in New Ipswich, NH.

²Ultra-high molecular weight polyethylene.

QUASI-STATIC TESTS AND REDESIGN OF CLAMPING SCHEME. Before attempting the dynamic impact tests, some of the materials and the clamping scheme were examined quasi-statically. We clamped a 6-in.-square piece of fabric into the mounting frame (see figure 7(b)), placed the frame into a press, and slowly pushed the 25-gram fragment simulator into the target while monitoring the ram pressure gauge.

The original clamping scheme was found to be of adequate strength for the felt targets. Figure 11 shows the deformation obtained in a 6-in.-square sample of a ultra-high molecular weight (UHMW) polyethylene felt (whose areal density of $\approx 0.03 \text{ g/cm}^2$ is similar to that of certain existing airplane insulation) after quasi-static deflection of $\approx 3.5 \text{ in.}$ The felt resisted the deflection with a force that ramped up to roughly 200 lb (900 N). The test was stopped when the force began to drop precipitously and the felt began showing obvious signs of imminent failure (see figure 11(a)). The test demonstrated that the felt could (at least quasi-statically) absorb a significant amount of energy in deformation before penetration by sustaining a moderate load for a substantial distance (our very rough estimate of the absorbed energy, based on our crude measurements for this test, was 34 J).

The original clamping scheme was not, however, found to be of adequate strength for the 2-D weave or layup targets. Even after adding more bolts to our clamping frame (to reach a total of 36, spaced approximately 0.7 in. around the perimeter) and tightening each bolt to the maximum possible before bolt failure ($\approx 100 \text{ in-lb}$ of torque), we could not prevent these fabrics from being pulled out of the frame at relatively low pressing forces well before fiber breakage.

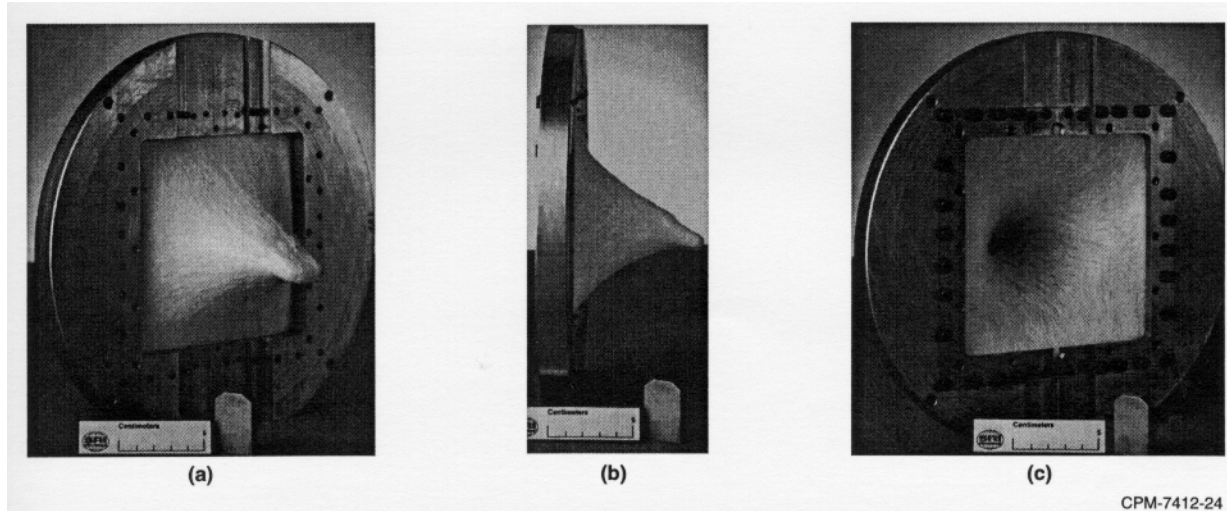


FIGURE 11. VIEWS OF UHMW POLYETHEYLENE FELT AFTER QUASI-STATIC DEFORMATION BY FRAGMENT SIMULATOR

The clamping scheme was redesigned to provide a stronger gripping force. The new scheme, shown in figure 7(c), involves wrapping the four ends of the fabric target (which is in the shape of a cross, with a 5-in.-square central region and 5-in.-wide extensions in the four directions) around steel rods and then clamping the fabric between a high-strength steel clamping frame, 90°-angle grooves cut into the backing frame, and three flattened faces on the steel rods. The clamping bolts (a total of 28, spaced approximately 0.8 in. apart) are larger than in the original device and can be tightened to 200 in-lb of torque. Before the bolts are tightened, the four free ends of the fabric are pulled taut to reduce slack in the target.

The new clamping scheme was tested quasi-statically with a Zylon target. The force on the impactor ramped up to ≈ 600 lb before a few of the fibers directly in front of the impactor snapped and continued up to ≈ 900 lb (at a deflection of roughly 1.5 in.) before the remaining fibers broke precipitously. Although there was some creep of the fabric at a couple of points along the frame, there was no rupture or pull out at the frame. Therefore, the clamping scheme proved successful.

IMPACT EXPERIMENTS—SINGLE-LAYER TARGETS. A second series of gas gun tests were performed in which our 25-gram Ti-6Al-4V fragment simulators impacted various high-strength fiber targets held by the clamping scheme described above. The targets were four of the materials described in table 6, including two of the three fabric types, the layups, the 2-D weaves, and all three of the fiber materials: aramid (TurtleSkin and Gold Shield), UHMW polyethylene (Spectra Shield), and PBO (Zylon).

Table 7 presents the relevant experimental parameters and results. The first four tests involved single-layer targets of the four materials, and the remaining three had multiple-layer targets. All of the tests resulted in full penetration. Figure 12 plots the energy absorbed during penetration versus the target's areal density for the four target materials.

TABLE 7. GAS GUN IMPACT TESTS USING HIGH-STRENGTH FABRIC MATERIALS

Test No.	Target			Areal Density (g/cm ²)	Impactor—Before Impact		Impactor—After Full Penetration		Kinetic Energy Lost (%)			
	Material Trade Name	Type of Fabric	Thickness per Layer		No. of Layers	Orientation of Layers ¹	Velocity (m/s)	K.E. (J)	Pitch ² (°)	Velocity (m/s)	K.E. (J)	Energy Lost (J)
13	Zylon	2-D weave	≈0.010 in.	1	0°	78	76	+3.6	29	10.5	65.5	86
14	TurtleSkin	2-D weave	≈0.011 in.	1	0°	78	76	-0.9	65.5	53.5	22.5	30
15	Spectra Shield	Layup	≈0.006 in.	1	0°	81.5	83	-8.1	72.5	66	17	20
16	Gold Shield	Layup	≈0.009 in.	1	0°	81.5	83	-7.1	69	60	23	28
17	Spectra Shield	Layup	≈0.006 in.	3	22°/0°/-22°	85	90	+2.2	50.5	32	58	65
18	TurtleSkin	2-D weave	≈0.011 in.	3	-22°/0°/22°	83.5	87	-15.6	40.5	20.5	66.5	76
19 ³	Zylon	2-D weave	≈0.010 in.	2	0°/22°	113	160	+35	64	51.5	108.5	68

¹ Orientations are measured clockwise from vertical. In each layer fiber plies are oriented both parallel and perpendicular to the orientation angle. For multiple layers, orientations are given in order from impact side to back side.

² As observed by camera in horizontal plane ("+" = nose down, "-" = nose up). For nonzero roll, it is a combination of pitch and yaw.

³ Data from this test are questionable because of the excessive pitch, debris from the aluminum honeycomb momentum trap traveling ahead of the impactor, and some PBO fibers from the back (22° orientation) layer breaking at the corner of the clamping rod and thus likely reducing the absorbed kinetic energy.

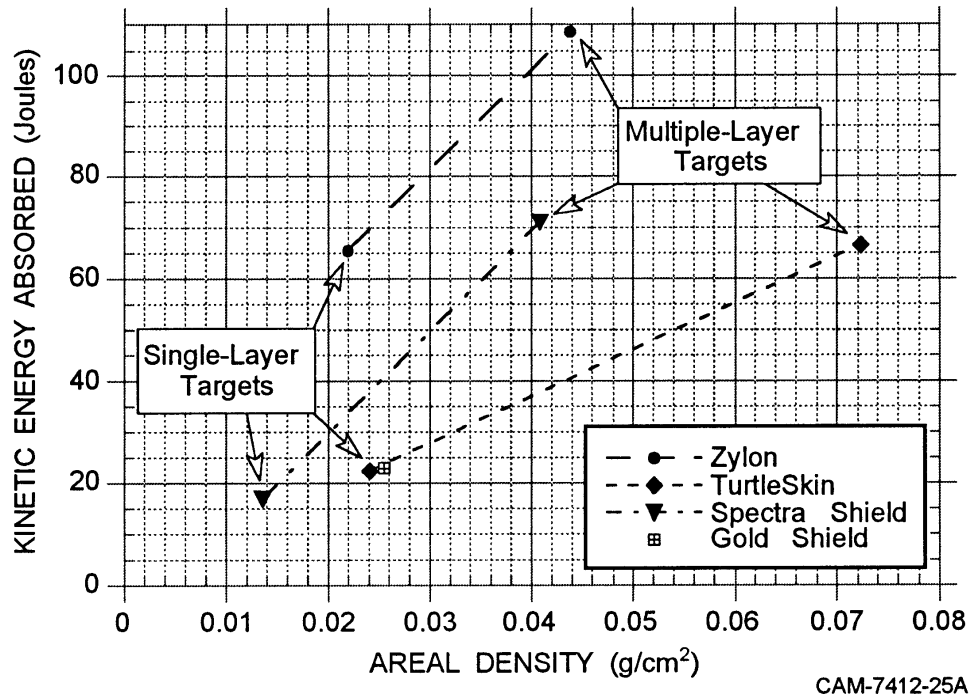
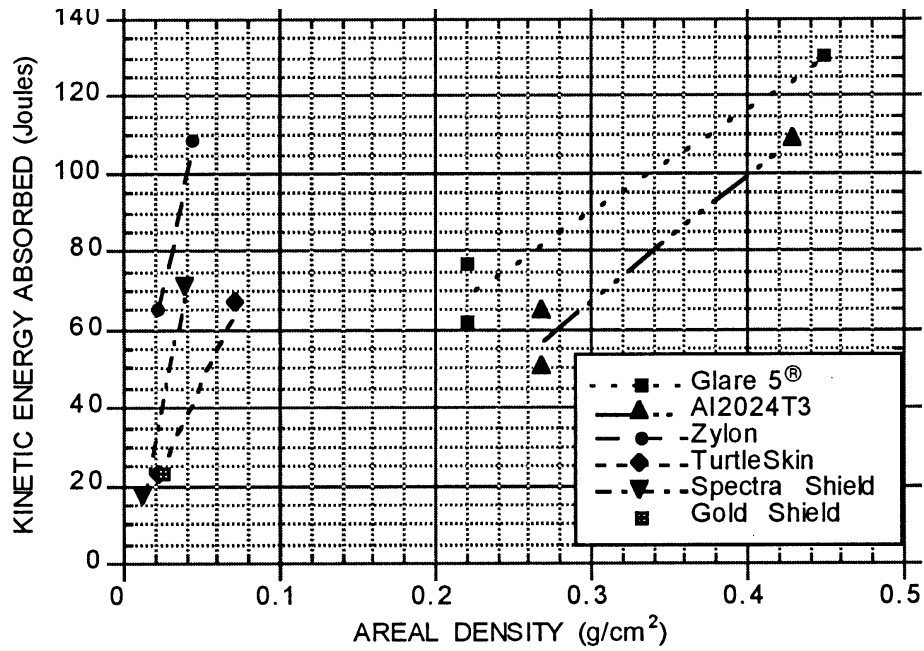


FIGURE 12. KINETIC ENERGY ABSORBED BY HIGH-STRENGTH FABRIC TARGETS DURING PENETRATION BY A 25-GRAM FRAGMENT SIMULATOR AT 80 m/s

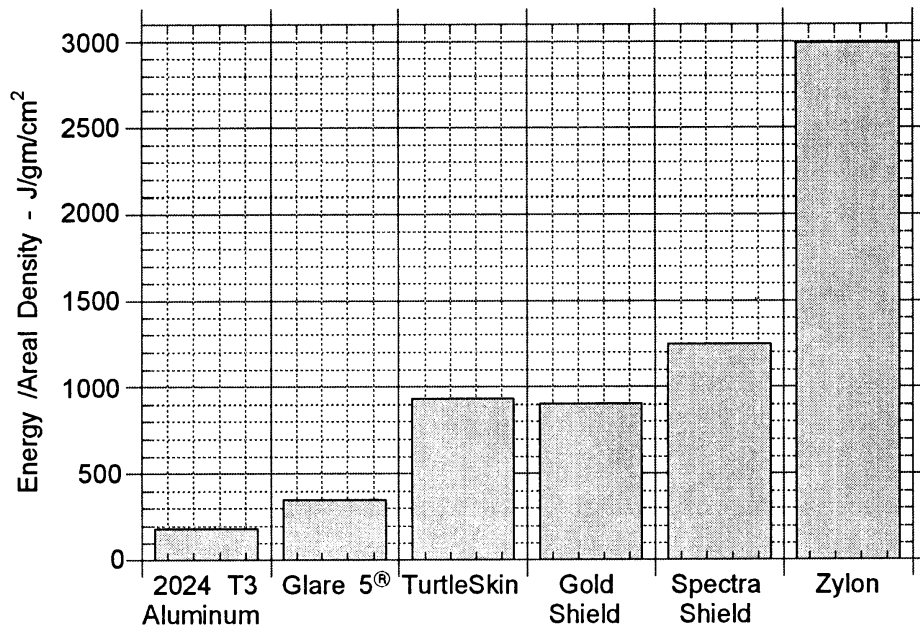
The four tests with the single-layer targets (Tests 13 through 17), all at an impact velocity of 80 ± 2 m/s, provide a good comparison of the energy absorption potential of the different materials. For the TurtleSkin, Spectra Shield, and Gold Shield targets the impactors lost from 17 to 23 J of kinetic energy (20% to 30% of their total) during penetration. For the Zylon target, however, the impactor lost 65.5 J of kinetic energy (86% of its total) during penetration. This result is quite remarkable, especially when compared with the results of the earlier tests with the aluminum materials (as shown in figure 13). The Zylon target, with an areal density of only 0.0219 g/cm^2 , absorbed more energy than the 2024-T3 aluminum target, whose areal density is 12 times higher.

In situations where total weight is critical, the figure of merit (or critical parameter) is energy absorbed per unit areal density. Figure 14 compares the energy absorbed per unit areal density for all six materials studied in this program (the two rigid and the four fabric materials) based on full-penetration tests with the 25-gram fragment simulator at velocities of 80 ± 2 m/s. The critical parameter for Zylon is 15 times that for 2024-T3 aluminum, nearly 9 times that for Glare 5[®] and at least 2.4 times that of the other fabric materials.



CAM-741226A

FIGURE 13 COMPARISON OF KINETIC ENERGY ABSORBED BY RIGID-WALL AND FABRIC TARGETS DURING PENETRATION BY A 25-GRAM FRAGMENT SIMULATOR AT 80 m/s



CAM-7412-27A

FIGURE 14. COMPARISON OF ENERGY ABSORBED PER UNIT AREAL DENSITY FOR FULL PENETRATION BY A 25-GRAM FRAGMENT SIMULATOR AT 80 m/s

PENETRATION MECHANISMS. We examined the recovered targets from the four single-layer impact tests to study the penetration mechanisms. Figure 15 contains photographs of the regions around the penetration holes for each of these tests. The two woven materials show significant differences (compare figures 15(a) and 15(e) with figures 15(b) and 15(f)). The Zylon shows substantial fiber displacement and disturbance of the fabric weave pattern in all four orthogonal directions from the point of impactor contact out to the clamping rod. The impactor appears to have punched through the TurtleSkin, however, disturbing the fabric only in the immediate vicinity of the penetration hole.

A rough measurement of how far the fragment displaced the fabric at the point of complete perforation can be obtained from the high-speed movies; they show the Zylon stretching about 20% farther than the TurtleSkin. This higher fabric displacement and the larger area of fabric deformation both likely contributed to the much larger absorption energy recorded for the Zylon than for the TurtleSkin, as did the higher fiber strength, as reported by the manufacturer (for PBO as compared with aramids or polyethylene).

Examination of the recovered targets from the two layup materials showed that they behaved qualitatively similarly: the fibers from both orthogonal plies that are in the region impacted by the fragment simulator's front face failed, and no other fibers were noticeably perturbed. The 0.25 x 0.50 in. rectangular gap in the Gold Shield (see figures 15(d) and 15(h)) is just the size of the impactor's front surface (see figure 6(b)); the horizontal fibers 0.25 in. above and below this gap simply moved aside as the diagonal portion of the 1.0-in.-wide impactor passed through and resumed their original location afterward. The wider gap for the Spectra Shield (see figures 15(c) and 15(g)) is likely due to a combination of impactor roll and/or yaw. The high-speed movies show the maximum fabric deformation for the two layups to be ≈ 0.25 in. less than for the TurtleSkin (≈ 0.45 in. less than for Zylon).

The horizontal and vertical plies in the Gold Shield were completely detached after the test, while those in the Spectra Shield were detached only in the region where the impactor had passed through. The Spectra Shield plies are more strongly bonded together than the plies of the Gold Shield before impact and remain largely bonded during penetration. This difference in bond strength may contribute to the result that the Spectra Shield absorbs only 30% less than the Gold Shield, while having only about half the areal density.

IMPACT EXPERIMENTS—MULTIPLE-LAYER TARGETS. For the three tests involving multiple-layer targets, we attempted to increase the energy-absorption potential of the multiple layers by orienting the layers at different angles. We would have liked to have used a 45° orientation for some of the layers, but then the fibers near the impact zone at the center of the target would extend outward toward the inside corners of the cross-shaped target, which are unclamped. So we selected $\pm 22.5^\circ$ as the orientation for some layers; impact zone fibers oriented at $\pm 22.5^\circ$ extend into the clamped region.

The results from the multiple-layer tests are shown in figure 12. With TurtleSkin and Spectra Shield, for which single-layer targets had absorbed less than one-quarter of the available kinetic energy, we used three layers in the targets and tested at impact velocities similar to those in the single-layer tests. The energy absorption for the three-layer TurtleSkin test was 3 times higher than that for the single-layer test. Whereas a 3-layer Spectra Shield test absorbed 3.4 times the

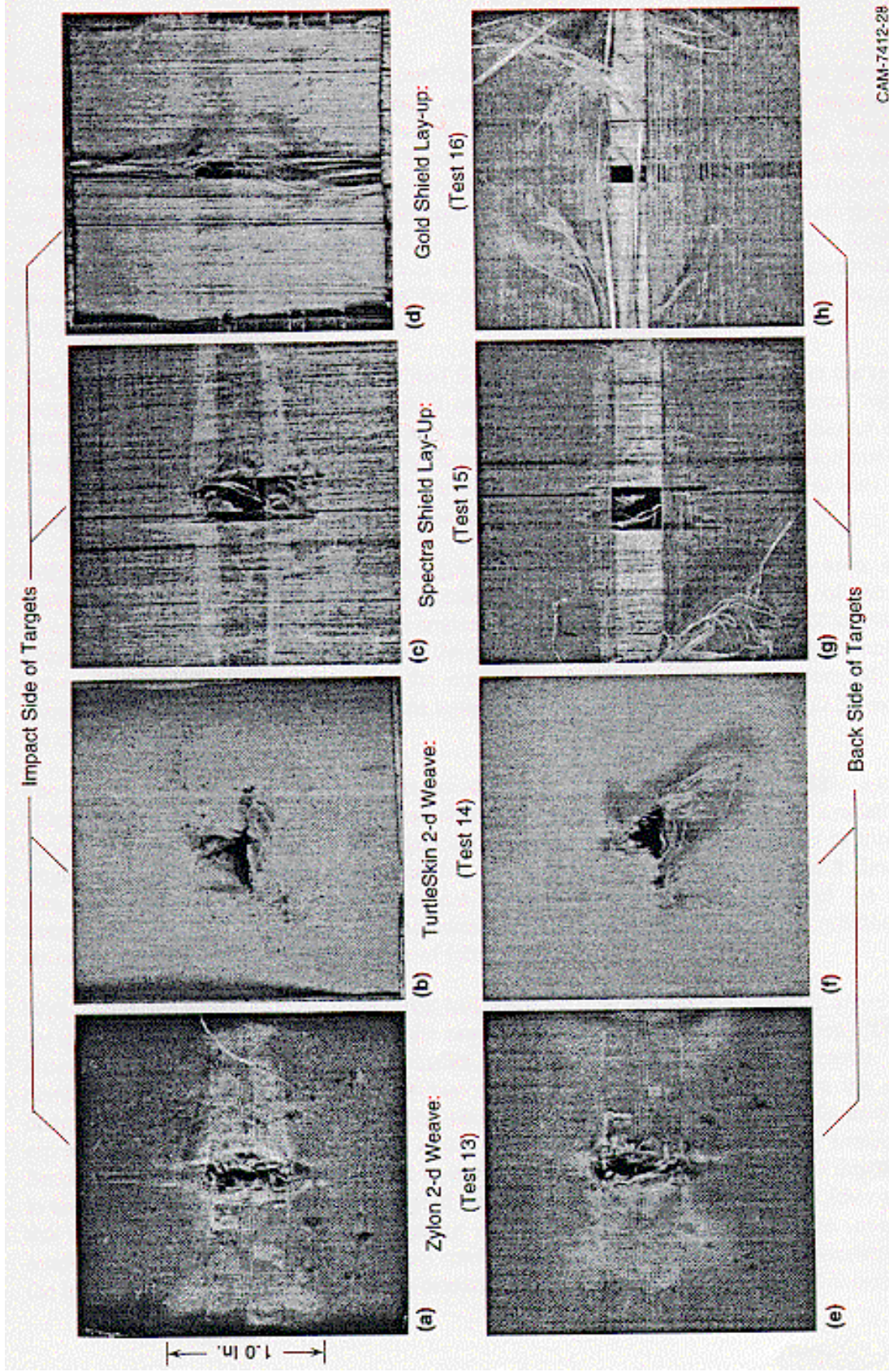


FIGURE 15. PHOTOS OF CENTRAL SECTIONS OF SINGLE-PLY FABRIC TARGETS RECOVERED AFTER IMPACT AND FULL PENETRATION BY A 25-GRAM FRAGMENT SIMULATOR AT 80 m/s

energy absorbed by a single layer. Additional tests are required to determine whether energy absorption is proportional to the number of fabric layers.

With Zylon, for which a single-layer target had absorbed over 86% of the available kinetic energy, we used only two layers and increased the impact velocity to ensure full penetration. The energy absorption increased by only $\approx 50\%$, smaller than the 100% increase in area density. But the results of this test are questionable for two reasons. First, some debris from the aluminum honeycomb being rapidly crushed between the sabot and the momentum trap (see figure 6) traveled out ahead of the target, impacting the target first and adding to the incoming kinetic energy. Second, some fibers from the rear Zylon layer (the layer with the 22.5° orientation) that were close to the impact zone impacted the very edge of one of the clamping rods, leading to fiber pull-out at that edge and thus weakening the response of that layer. This test should be repeated with modifications to the sabot/momentum trap configuration to better contain the honeycomb debris at the higher impact velocities and with the orientation of the rear Zylon fiber reduced to perhaps 15° .

DISCUSSION AND CONCLUSIONS. These few tests do not necessarily demonstrate that a particular fiber material (e.g., the PBO in Zylon) is superior to the other fiber materials or that a particular fabric type (e.g., the 2-D weave) is superior to other fabric types in terms of kinetic energy absorption during a fragment penetration, because all of the four fabrics we used had different structures. The TurtleSkin, for example, has a much tighter weave than the Zylon and uses fibers of smaller diameter. The Spectra Shield uses thinner fibers than the Gold Shield, but holds these fibers together more tightly. Although the results suggest that PBO is the best of the fiber materials currently available, and that a 2-D weave can absorb more energy than a layup, further tests are needed to confirm these indications and to optimize the fiber diameter, tightness of weave, and other fabric design parameters to maximize the energy absorption potential.

What these tests have definitively demonstrated is that high-strength fabric materials do have a very large fragment energy absorption potential per unit areal density and thus should be strongly considered in fragment barrier designs where minimizing the weight is important.

FINITE ELEMENT CALCULATIONS. We performed finite element calculations to simulate two of the gas gun tests of a titanium impactor on a 6-in.-square aluminum target. The main objective of these calculations was to evaluate our ability to calculate the response of fragment barriers, including damage and failure of the barrier. The long-term goals of the calculational program are to use finite element calculations to analyze and understand fragment barrier impact experiments and to use the insights gained from the calculations to provide feedback to experiments; for example, to investigate barrier design concepts. We envision that these calculations will enable us to identify important parameters in the barrier design and to determine the dependence of barrier effectiveness on various design parameters such as spacing, angles, and materials and to help improve and optimize barrier designs.

Our approach was to use the DYNA3D⁽⁴⁴⁾ finite element code to perform the simulations. DYNA3D is a nonlinear, explicit, three-dimensional nonlinear finite element code for analyzing the dynamic response of structures. DYNA3D calculates failure in materials using a tied node with failure (TNWF) algorithm for shell elements.⁽⁴⁴⁾ In the TNWF algorithm, a strain to failure

is specified for the material. When the averaged value of effective plastic strain for elements connected at a nodal location reaches the specified value, the nodes are released and allowed to move independently. The appendix gives the input files for these fragment impact calculations.

The materials were modeled as elastic plastic with strain hardening. We used handbook values for the material properties of the Ti-6Al-4V titanium impactor and the 2024-T3 aluminum target, listed in table 8. We included a value of strain to failure of 0.20 for the aluminum.

TABLE 8. MATERIAL PROPERTIES USED IN FINITE ELEMENT IMPACT SIMULATIONS

	Ti-6Al-4V	2024-T3 Al
Young's modulus	110 GPa (16 x 10 ⁶ psi)	69 GPa (10 x 10 ⁶ psi)
Poisson's ratio	0.30	0.33
Yield strength	827 MPa (120 ksi)	345 MPa (50 ksi)
Hardening modulus	2.1 GPa (3.0 x 10 ⁵ psi)	0.69 MPa (1.0 x 10 ⁵ psi)
Weight density	4.47 g/cc (0.16 lb/in. ³)	2.7 g/cc (0.10 lb/in. ³)
Strain to failure		0.20

The configuration for the calculations is shown in figure 16. The target is a 15.24-cm-square (6.0-in.), 1.0-mm-thick (0.040-in.) sheet of aluminum. A 9.5-mm (3/8-in.) fixed border was included on all sides of the target. The impactor was a 25.2-gram titanium impactor with dimensions as shown in figure 6(b). The finite element mesh contained about 2,000 eight-noded brick elements for the impactor and over 12,000 shell elements for the target. The impactor was given an initial velocity and initial position (i.e., specified pitch and roll angles) as measured in the experiment.

We performed simulations of an experiment close to the ballistic limit, Test 3, and an experiment well above the ballistic limit, Test 6. For Test 3, the impactor velocity at impact was measured at 59 m/s with a pitch angle of -13.3° and a roll angle of -10.0°. The results for Test 3 showed partial perforation of the target. Because Test 5 at slightly lower impact velocity (56 m/s) showed deformation only, we consider Test 3 to be just slightly above the threshold for penetration.

The results of the DYNA3D simulation of Test 3 are shown in figure 17. Figure 17(a) shows fringes of velocity in the plate and impactor at 60 μs. At this early time, the impactor velocity has slowed only slightly to about 50 m/s, and the plate has begun to deform in concentric circles around the impactor. At 380 μs, shown in figure 17(b), the impactor has slowed considerably, to about 10 m/s, and the fringe patterns of velocity in the plate show the effects of the square boundary. At 790 μs, shown in figure 17(c), the impactor has rebounded from the plate, with a rebound velocity of about 20 m/s. The calculated damage in the plate shows permanent deformation at the impacted location and several elements near failure, but no perforation of the plate was calculated. The calculated rebound velocity of 20 m/s was somewhat greater than the measured rebound velocity of 15.3 m/s.

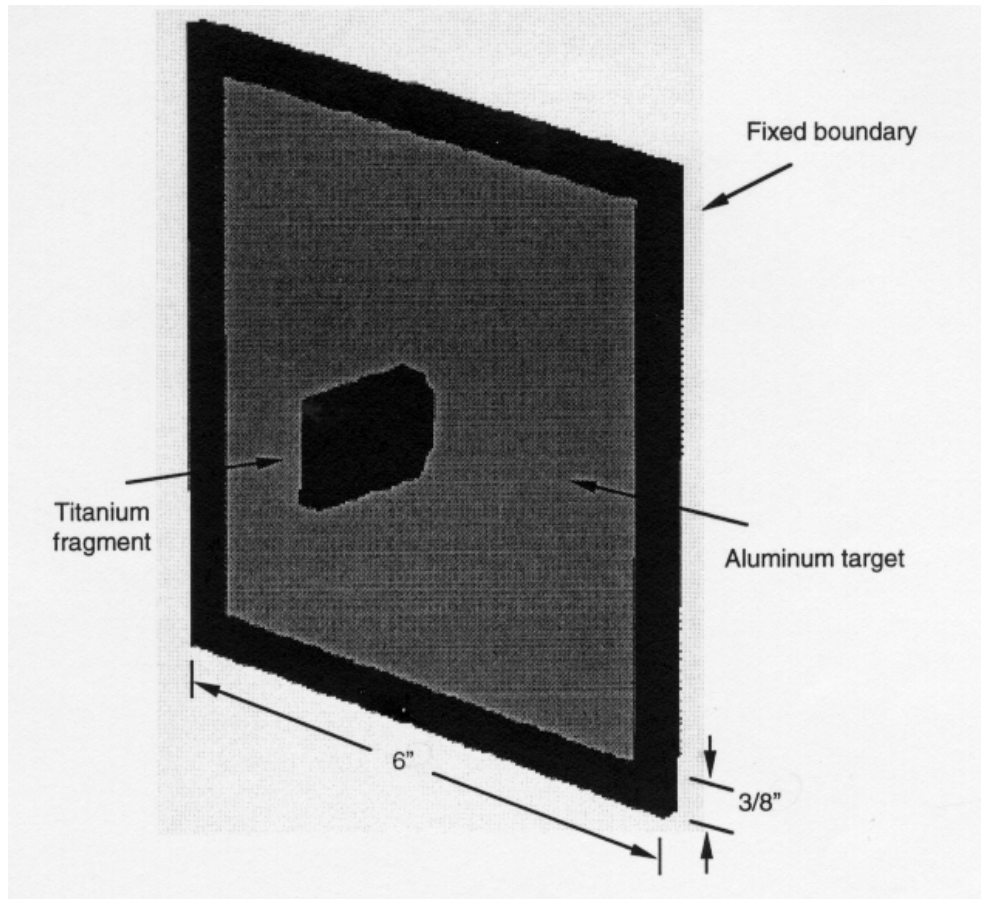


FIGURE 16. DYN3D CONFIGURATION FOR FRAGMENT SIMULATOR CALCULATIONS

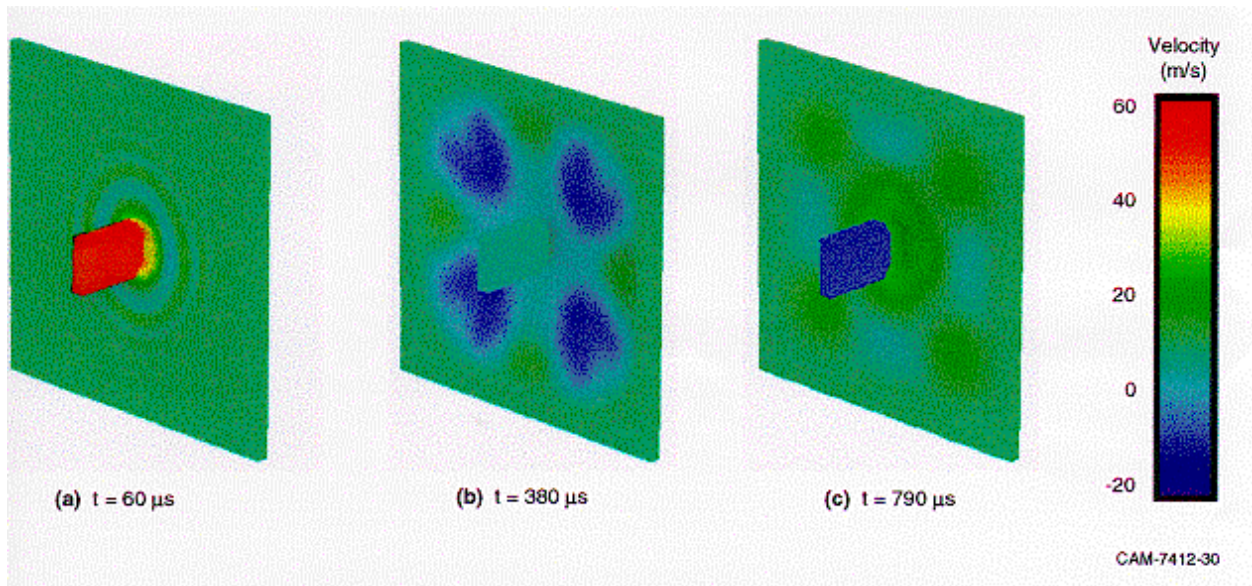


FIGURE 17. DYN3D CALCULATED RESULTS FOR TEST 3, IMPACT VELOCITY 59 m/s

measured at 95 m/s with a pitch angle of -9.3° and a roll angle of -9.5° . The target for Test 6 was completely penetrated by the impactor. The results of the DYNA3D simulation of Test 6 are shown in figure 18. Figure 18(a) shows fringes of velocity in the plate and impactor at $40 \mu\text{s}$. The impactor velocity has slowed very little and the plate shows circular ripples in velocity. At $100 \mu\text{s}$, shown in figure 18(b), the impactor has slowed to about 75 m/s and has begun to penetrate the target. The fringe patterns of velocity in the plate still show circular velocity patterns. At $250 \mu\text{s}$, shown in figure 18(c), the impactor fully penetrated the plate and has a residual velocity of 65 m/s, which is slightly higher than the measured residual velocity of 61.8 m/s.

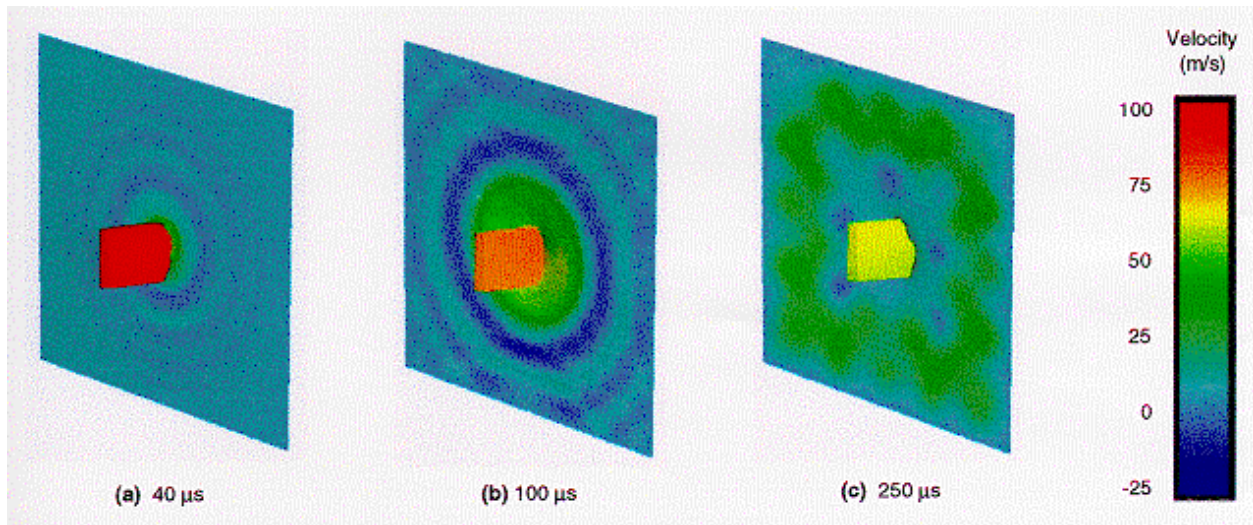


FIGURE 18. DYNA3D CALCULATED RESULTS FOR TEST 6, IMPACT VELOCITY 95 m/s

These two simulations demonstrate the capability for using DYNA3D to calculate the impact response of target materials including damage and failure. The simulations showed good overall agreement with the experimental results. The results of the Test 3 simulation indicate that 59 m/s is very near the threshold velocity for this target and penetrator. This is a good result considering that we used handbook values for the mechanical properties of the titanium and aluminum.

The discrepancies between the experiment and simulation, that the experiment showed slight perforation and lower rebound velocity than the simulation, could be due to differences in the actual material properties for the target material or in simulation assumptions, for example, that the boundaries were rigid. There may have been slight slippage in the experiment that was not modeled in the simulation. The simulation of Test 6 demonstrates the ability to calculate target response well into the regime of material failure.

THE NEXT STEPS

To achieve a practical fragment barrier design for aircraft, we recommend that two efforts be undertaken simultaneously:

1. A semiempirical effort in which the ballistic effectiveness of the materials and barrier designs identified in this work is evaluated in tests against simulated fragments and the designs are modified to achieve acceptable protection.
2. A semicomputational effort in which a fragment-barrier impact simulation capability is developed that can be used for parametric investigations and barrier design optimization.

The semiempirical effort should result in acceptable barriers in the short term; the semicomputational effort should result in more efficient barriers in the long term.

Each effort requires both experiments and computations. In the experiment-dominated effort, time to implementation is emphasized at the expense of some weight and cost efficiencies. In the computation-dominated effort, more efficient barriers are anticipated, but they will not be available until a later time.

NEAR-TERM ENGINE FRAGMENT BARRIERS.

To achieve practical engine fragment barriers in the near term, barrier designs using high-strength fabrics as described in this work should be assembled and their ability to defeat impinging fragments determined. The ballistic performance of various weaves, felts, and layups of aramids, polyethylenes, and PBO should be evaluated in gas gun tests with simulated fragments in which absorbed energy is measured. These results should be used to rank the materials and fabrics, to determine required thicknesses, and to innovate modifications to the designs.

The impacted barriers should be examined macroscopically and with a scanning electron microscope to determine damage mechanisms of the component materials and structures. Such information is useful in designing improved barriers and in choosing or developing mathematical models that describe damage evolution.

The results of the tests should be input into the existing DYNA capability, and the impact response of the modified designs should be simulated. Further computational simulations should be performed to assist the understanding of barrier parameters such as physical and mechanical properties of barrier components, layer thicknesses, interface bond strengths, spacings, and angles. Based on the findings, and as warranted, the barriers should be further modified, assembled, and tested.

This iterative procedure of impact experiments and computations is repeated until a barrier system having acceptable ballistic performance, weight, and cost is achieved.

Minimizing aircraft tare weight requires that the barriers perform functions of, and hence replace, currently used structures. Within the fuselage wall, these structures include the interior paneling and the fiberglass insulation blanket. Thus, the materials and fabrics that emerge as likely barrier

components should be evaluated for their abilities to provide thermal and acoustic insulation and for their water absorption and flame resistant properties. Structural solutions should be pursued to address nonballistic function issues (i.e., tough fabrics as water barrier envelopes for the felts).

A key issue is how to attach the barriers to the structural members of the fuselage. The barriers will be most effective if attached firmly to these members, so that when impacted, fibers in the barriers experience maximum stress and hence exert maximum slowing force on a fragment before tearing away. Large area barriers that span many structural grids will cause a greater number of structural members to be involved in slowing fragments and thus may also be desirable. At cross purposes is the desirability that the barriers be easily removable during teardown inspections.

The energy absorption capability of the structural members of the fuselage skeleton (frame members and longerons) should be evaluated in gas gun impact tests. Possible failure modes for individual members are penetration and plastic hinging, which will depend on the size, shape, and velocity of the projectile. Structural collapse of a section of the skeleton will be another failure mode if large area barriers or strongly attached barriers are used.

A COMPUTATIONAL DESIGN/EVALUATION CAPABILITY.

Although the semiempirical approach discussed in the preceding paragraphs could result in practical engine fragment barriers in a short time, the barriers will most probably not be optimal in terms of weight, space, and cost. To achieve more efficient barrier designs, a computational capability should be developed that can simulate various fragment-barrier impact scenarios and predict the outcome with some reliability. Such a capability would allow the influence on ballistic effectiveness of the many parameters of the barrier structures and the impact scenarios to be determined in a cost-effective way and implicate superior barrier designs, which then could be investigated and validated in a much more limited series of impact experiments.

The computational capability would consist of a computer code (which calculates the distribution and history of stresses and strains in the fragment and barrier), a deformation and failure model(s) (which describe how the materials respond to the stresses and strains), and constitutive data and failure criteria (measured in laboratory tests for the specific materials of interest, which quantify the models). The status of these elements is summarized in the following paragraphs.

COMPUTER CODES. Advanced, nonlinear, dynamic, computer analysis codes are needed to calculate stresses, strains, and damage in projectiles and targets at all locations and at all times during a ballistic impact event. Many commercially available finite element codes can treat impact/penetration scenarios and accept material and failure models. The most suitable codes appear to be AUTODYNE, DYNA3D, DYTRAN, LS-DYNA, and STARDYNE.

DEFORMATION AND FAILURE MODELS. Mathematical descriptions of the deformation and failure characteristics of the impacting and impacted materials are needed to compute the response of the materials to the ballistic loads. For homogeneous materials, the most widely used deformation models are Johnson-Cook (empirical), Zerilli-Armstrong (dislocation-mechanics-based), and Bodner-Partom (specialized for impact). Parameters for J-C and B-P are determined from fits to data (J-C parameters exist for about 27 materials); Z-A parameters can be estimated from first principles. Over 90% of composite structure designers use either maximum stress,

maximum strain, or quadratic polynomial theories for failure criteria. For composites and textiles, consensus deformation and failure models are lacking.

HIGH STRAIN RATE CONSTITUTIVE DATA. Measurements of the deformation produced by an applied load are needed to quantify a material model. Stress-strain curves in tension, compression, and shear as a function of strain rate and temperature exist for many metallic, ceramic, polymeric, and composite materials. In general, homogeneous materials are the best characterized, ceramic materials show little rate dependence, composites are characterized as continua, and polymer fibers are poorly characterized at high strain rates.

HIGH STRAIN RATE TEST TECHNIQUES. Mechanical tests are needed to measure constitutive and failure behavior of materials under various states of stress at elevated strain rates. High strain rate tests exist, but no test is standard. Furthermore, no test is capable of measuring behavior over the entire dynamic range of strain rates or stress states; thus, a comprehensive characterization of a material requires that several types of tests be performed. Finally, no reliable test currently exists for determining the high strain rate behavior of fibers.

SUMMARY.

The state of the art in computational penetration analysis is advanced and is progressing, and a strong basis exists for developing a computational fragment-barrier impact simulation capability. Existing finite element codes appear adequate for simulating the impact of a fragment with a barrier. Deformation and failure models and data exist for many steels, aluminum alloys, titanium alloys, and other homogeneous materials and are often adequate for penetration computations. Most of the current candidate armor ceramics have been recently well characterized with respect to static properties, and because these materials exhibit little strain rate dependence, these data may adequately describe ballistic behavior.

However, several information gaps prevent reliable simulations of ballistic response of certain materials, especially those polymeric materials identified in this work as most promising for engine fragment barriers on aircraft. Models and data for composites tend to be empirical, based on continuum assumptions, and situation dependent. For fibers and textiles, modeling efforts are scattered, the phenomenology of projectile impact is poorly understood, high strain rate data are scarce, and reliable test techniques for measuring ballistic response do not exist. The diagnostic and analysis capabilities available today should allow these current shortcomings to be overcome.

CONCLUSIONS

REVIEW OF MILITARY ARMOR TECHNOLOGY.

Our survey of the advanced armor materials included metallic alloys, ceramics, polymers, and composites. In assessing their potential for implementation on aircraft, we considered material weight, cost, and ancillary properties, in addition to mechanical properties and ballistic performance.

We concluded that highly ordered, highly crystalline, high molecular weight polymers, because of their low density and high strength, hold great promise for engine fragment barriers on aircraft.

Specifically, fibers of certain aramids, polyethylenes, and polybenzoxazole (PBO) appear capable of providing a useful measure of ballistic protection in the most weight-efficient manner. These materials can be configured as weaves, braids, knits, layups, felts, and as components of reinforced resins, providing extensive design flexibility in achieving weight-efficient barriers.

The survey further showed that advanced ceramics should be considered as components in aircraft armor. Great strides were made during the recent DOD armor initiative in understanding and characterizing the ballistic performance of ceramics. In particular, encapsulated tiles of Al_2O_3 , SiC, B_4C , TiB_2 , AlN, and certain ceramic alloys and cermets were shown to be effective in defeating projectiles at areal densities significantly lower than their metallic counterparts.

As regards metallic materials, the strength and toughness of aluminum alloys, titanium alloys, and steels have been enhanced in recent years by compositional changes, thermomechanical treatments, and improvements in cleanliness. Gains in ballistic resistance, however, have been only marginal. Nevertheless, these newer alloy variants may find application within the nacelle. Metal matrix and ceramic matrix composites were little used in battle tank armor.

BARRIER DESIGN FOR ENGINE FRAGMENTS.

Based on the findings from the DOD armor review, a fragment barrier scheme was conceived for preventing low energy fragments from penetrating the fuselage wall and then severing control lines or damaging a second engine. The scheme consists of felts and multilayers of high strength polymer fibers with to-be-specified spacing and boundary conditions. The barrier scheme seeks to minimize added weight and cost by replacing existing materials in the fuselage wall with dual function ballistic materials.

A second scheme uses an inclined laminate of polymer, ceramic, and metal alloy to provide local protection to fuel and control lines.

FRAGMENT BARRIER TEST FACILITY.

A fragment impact test facility was designed, constructed, and used to begin to evaluate the ballistic resistance of fuselage wall materials and several advanced materials. A fragment-simulating projectile was designed, a gas gun was modified to accelerate the projectile against a barrier at prescribed velocity, and a high-speed camera was positioned to record impact and residual velocities, allowing absorbed energy to be determined. Against a 25-gram simulated fragment at 80 m/s glass fiber-aluminum laminates absorbed nearly twice the energy absorbed by conventional aluminum fuselage skin of equivalent weight. Strong polymer fibers, tested as layups and weaves, however, absorbed much higher energies and in terms of aerial density were 5 to 10 times more efficient than aluminum fuselage skin, suggesting that these materials will perform well as components of aircraft fragment barriers.

COMPUTATIONAL SIMULATIONS.

A computational tool for interpreting impact experiments and designing barriers was developed. A tied-node-with-failure algorithm introduced into the material failure model used in the DYNA3D code enables us to estimate the residual velocity of a penetrating fragment and thus evaluate the energy-absorbing capacity of potential barrier systems. Computed results on

aluminum aircraft skin agreed well with experiments; more complex failure models and high strain rate material properties are needed to apply the tool to polymer fibers.

RECOMMENDATIONS

This work has confirmed high-strength polymer fibers as the advanced material most appropriate for protecting aircraft from engine fragments and has identified three particular polymers as having the prerequisite low density and high strength. Polybenzoxazole, because of its exceptional ballistic properties, flame resistance, and water absorption resistance, appears to be particularly suited as a barrier material. The next step is to design practical barriers from these fibers that can meet the aircraft requirement for flame and water resistance, along with thermal and acoustic insulation properties.

Much design flexibility exists because the three fiber types can be produced in many diameters, lengths, and surface finishes; the fibers can be configured in many types of weaves, felts, and layups; and these configurations can be assembled in many geometries, fiber mixes, and can include other materials.

We recommend two efforts be undertaken to capitalize on these findings: a semiempirical effort to evaluate the ballistic effectiveness of existing polymer fabric structures and barrier designs, and an effort to develop a computational capability for designing and evaluating barrier schemes based on material failure mechanisms and properties. The former effort could result in acceptable barrier systems in the near term; the latter aims for the longer-term is the design of barrier systems more optimal in terms of weight, cost, and ease of installation and removal for aircraft inspections. These efforts can be performed simultaneously.

REFERENCES

1. Aircraft Catastrophic Failure Prevention Research Program, Program Plan, DOT/FAA/CT-94/26, January 1994, U.S. Department of Transportation, Federal Aviation Administration, Technical Center, Atlantic City International Airport, NJ (1994).
2. The DARPA/Army/Marine Corps Armor/Antiarmor Program, 1986-1993, Patrick Sullivan, Program Manager, Defense Advanced Research Projects Agency, Arlington, VA.
3. F. S. Mascianica, "Ballistics Technology of Lightweight Armor-1981," Army Materials and Mechanics Research Center Technical Report AMMRC TR 81-20, Watertown, MA (May 1981) (confidential).
4. DARPA Classification Guide SCG-117.
5. T. A. Havel, Armor Mechanics Branch, U.S. Army Research Laboratory, Aberdeen Proving Ground, MD 21005.
6. Classification Guide, 30 July 1993.
7. O. D. Sherby, B. Walser, C. Young, and E. Cady, "Superplastic Ultra-High Carbon Steels," *Scripta. Met.*, **9**, 569 (1975).
8. R. D. Caligiuri and L. E. Eiselstein, private communication, SRI International, Menlo Park, CA 94025.
9. K. McHenry, private communication, Alliant TechSystems, Inc., Hopkins, MN 55343.
10. R. Heiple and Kornish, private communication, ALCOA Technical Center, Alcoa Center, PA 15069.
11. Final Technical Report to the Defense Advanced Research Projects Agency on Contract N60921-85-C-A010, 1987 by Reynolds Metals Company, Corporate Research and Development, Corporate Technology Center, 13203 N. Enon Church Road, Chester, VA 23831-3122.
12. J. C. Fanning, "Terminal Ballistic Properties of *TIMETAL*[®] 62S," presented at the Eighth World Conference on Titanium, Birmingham, United Kingdom (October 22-26, 1995).
13. J. E. Drotleff and R. Musante, private communication, United Defense, San Jose, CA.
14. D. Viechnicki, W. Blumenthal, M. Slavin, C. Tracy, and H. Skeelee, Armor Ceramics: 1987 Third Armor Coordinating Conference, February 17-19, 1987, Monterey, CA.
15. M. Kliman and M. Slavin, "Comparative Mechano-Ballistic Evaluation of Alpha Silicon Carbide/Titanium Diboride Structures," Proceedings of the Fourth Tacom Armor Coordinating Conference for Light Combat Vehicles, March 29-31, 1988, Volume II.
16. R. L. Landingham and A. W. Casey, "Final Report of the Light Armor Materials Program," UCRL-51269 (September 15, 1972).

17. M. L. Wilkins, C. F. Cline, and C. A. Honodel, "Light Armor," UCRL - 71817 Lawrence Radiation Laboratory, University of California, Livermore, CA (July 23, 1969).
18. M. L. Wilkins, "Computer Simulation of Penetration Phenomena," Chapter 10 in *Ballistic Materials and Penetration Mechanics*, R. C. Laible, Ed. (Elsevier, 1980).
19. M. Mayselless, W. Goldsmith, S. P. Virostek, and S. Finnegan, "Impact on Ceramic Targets," *J. Appl. Mech.*, **54**, 373 (1988).
20. Yasiv, G. Rosenberg, and H. Shevah, "Parametric Study of Ceramic Laminated Armor Configurations," *Armor Ceramics: 1987 Third Armor Coordinating Conference*, February 17-19, 1987, Monterey, CA.
21. B. Scott, private communication, DuPont Company, P.O. Box 80,0705 Laurel Run, Wilmington, DE 19880-0705.
22. D. J. Viechnicki, M. J. Slavin, and M. I. Kliman, "Development and Current Status of Armor Ceramics," *Ceramic Bulletin* **70** (6), 1035-1039, 1991.
23. R. Palicka, SiC Properties, Proceedings of the 9th Ceramic Modeling Working Group, November 4-5, 1992, Institute for Advanced Technology, University of Texas, Austin, TX.
24. J. F. Wolfe, P. D. Sybert, and J. R. Sybert, U.S. Patent 4533693 (1985).
25. "High Performance Structural Fibers for Advanced Polymer Matrix Composites," National Materials Advisory Board, 2101 Constitution Avenue, NW, HA-262, Washington, DC 20418.
26. H. H. Yang, *Kevlar Aramid Fiber* (John Wiley & Sons Ltd., Baffins Lane, Chichester, England, 1993).
27. K. Shariq, E. Anderson, and Y. Sakuma, "Specialty Organic Fibers," *Chemical Economics Handbook*, SRI International, Menlo Park, California (1995).
28. K. Leighton, private communication, Lanxide Armor Products, Inc., 1300 Marrows Road, P.O. Box 6077, Newark, DE 19714-6077.
29. W. B. Scott, "New Ceramic Armor Protects Crews on Peacekeeping Flights," *Aviation Week and Space Technology*, a publication of the McGraw-Hill Companies (July 17, 1995).
30. United Defense Ground Systems Division, 1107 Coleman Avenue, Box 367, San Jose, CA 95103.
31. K. Shariq, E. Anderson, and Y. Sakuma, "Specialty Inorganic Fibers," *Chemical Economics Handbook*, SRI International, Menlo Park, California (1996).
32. C. Frankenberger and J. K. Manion, "Uncontained Engine Debris Damage Mitigation Program," FAA Interagency Agreement No. DTFA03-95-X-90019, Naval Air Warfare Center Weapons Division, China Lake, CA 93555.

33. D. Tilzey, "Uncontained Engine Debris Trajectory Study," Boeing Company, BCAG Propulsion Research BNR04, Document No. D6-57019-1 (September 1995).
34. C. Lewis, private communication, Boeing Commercial Aircraft Group, Seattle, WA.
35. C. O. Gunderson, "Study to Improve Airframe Turbine Engine Rotor Blade Containment," Federal Aviation Administration Technical Report (FAA RD 77-44, Contract No. DOT FA76WA-3843), Washington, DC (1977).
36. National Transportation Safety Board, "Aircraft Accident Report," PB90-910406, NTSB/AAR-90/06 (July 19, 1989).
37. Preliminary National Transportation Safety Board write up, Delta Air Lines, Inc. Accident Occurred July 6, 1996 at Pensacola, FL (NTSB Identification: DCA96MA068—the docket is stored in the (off-line) NTSB Imaging System) (1996).
38. National Transportation Safety Board, Aircraft Accident Report No. NTSB/AAR-96/03, "Operation of ValuJet Airlines, Accident Occurred June 8, 1995 at Atlanta, GA," (NTSB Identification: ATL95MA106—the docket is stored in the (off-line) NTSB Imaging System (1996).
39. A. D. Lane, "Development of an Advanced Fan Blade Containment System," National Aeronautics and Space Administration Final Report (Report No. N90-13386/9/XB) (August 1989).
40. J. J. DeLuca and S. P. Petrie, "Evaluation of Lightweight Material Concepts for Aircraft Turbine Engine Rotor Protection," *Advanced Materials: Looking Ahead to the 21st Century* (Boston, MA, 1990) pp. 319-333.
41. J. Pepin, "Fiber Reinforced Structures for Small Turbine Engine Fragment Containment (Phase II)," report by Pepin Associates, Inc. (DOT/FAA/AR-95/110, July 1996), Scarborough, ME.
42. D. J. Gartland and M. P. Miller, "Design and Assessment of Airplane and Engine Systems to Minimize Engine/Failure Hazards," PROP-BN86P-P94-001, Boeing Commercial Airplane Group (1994).
43. C. L. Stotler, "Development of Advanced Lightweight Containment Systems," Final Technical Report No. NASA CR-165212, prepared by General Electric Company, Cincinnati, OH (1981).
44. R. G. Whirley and B. E. Engelmann, "DYNA3D A Nonlinear, Explicit, Three-Dimensional Finite Element Code for Solid and Structural Mechanics—User Manual," UCRL-MA-107254 Rev. 1, Lawrence Livermore National Laboratory, Livermore, California (November 1993).

APPENDIX A—INGRID AND DYNA3D INPUT FILES FOR THE FRAGMENT IMPACT CALCULATIONS

This appendix contains listings of the INGRID and DYNA3D input files for a representative fragment impact simulation performed in this study. The INGRID program is the preprocessor used for the mesh and model generation. DYNA3D is the nonlinear dynamic finite element code used in the analyses. Additional information on each of the input files and model generation is given below.

INGRID INPUT FILE.

The following is the complete listing of the INGRID input file used to create the final version of the DYNA3D fragment impact model input file. This INGRID input file generates the complete DYNA3D model with the exception of the tied node with failure algorithm used to simulate the fragment penetration. These tied node input cards were generated using a simple program that searches the nodal positions, finds nodes at coincident locations, and writes the input cards in the proper format. The tied failure algorithm also requires input of a failure strain, which was set at 20% for these simulations.

Alternatively, this model could be modified to run without the failure by specifying a part tolerance for the discrete element zone that is a positive number.

```

FRAG1 - fragment penetration calculation
dn3d
c
term 1.00e-03
prti 1.00e-04
plti 2.50e-05
tssf 0.70e+00
pnlt 1.00e-02
c
c plane 1
c 0.0 0.0 0.0    0.0 1.0 0.0  0.0001  symm
c
c          global coordinate transformation
c
c gct 3 ; my 0.50 ; mz 0.50 ; my 0.50 mz 0.50 ;
c
c          sliding interfaces
c
c si 1 sv ;
c
c          part definitions
c
start                c part 1 - fragment
  1 15 ;
  1 5 13 17 ;
  1 5 ;
  0.000 1.260
 -0.500 -0.250  0.250  0.500
 -0.125  0.125
c
mb 2 2 1 2 3 2    1  0.175
c
sii  -2 ; 1 4 ; 1 2 ; 1 s
sii  1 2 ; -1 -4 ; 1 2 ; 1 s
sii  1 2 ; 1 4 ; -1 -2 ; 1 s
c
coor 1 ; rz 0.0 rx 2.4 ;
lrep 1 ;
c
velocity 2.323e+03  0.000  0.000
c
mate 1
end
c
c
start                c part 2 - outer frame
  1 2 3 ;
  1 4 11 91 98 101 ;
  1 4 11 91 98 101 ;
  1.400 1.500 1.600
 -3.000 -2.625 -2.000  2.000  2.625  3.000
 -3.000 -2.625 -2.000  2.000  2.625  3.000
c
di  1 3 ; 2 5 ; 2 5 ;
c
b 1 1 1 3 6 1  111111
b 1 1 6 3 6 6  111111
b 1 1 1 3 1 6  111111
b 1 6 1 3 6 6  111111
b 3 1 1 3 2 6  111111
b 3 5 1 3 6 6  111111
b 3 2 1 3 5 2  111111
b 3 2 5 3 5 6  111111
c
velocity 0.0 0.0 0.0

```

```

c
mate 1
end
c
c
start                c part 3 - outer shell
-1 ;
  1 4 11 91 98 101 ;
  1 4 11 91 98 101 ;
  1.50
  -3.000 -2.625 -2.000  2.000  2.625  3.000
  -3.000 -2.625 -2.000  2.000  2.625  3.000
c
  di  -1 ; 3 4 ; 3 4 ;
c
c  b 1 1 1 1 6 1  111111
c  b 1 1 6 1 6 6  111111
c  b 1 1 1 1 1 6  111111
c  b 1 6 1 1 6 6  111111
c
c sii  -1 ; 2 3 ; 2 3 ; 1  m
c
  velocity 0.0 0.0 0.0
c
thick 0.040
mate 2
end
c
c
start                c part 4 - shell break area
-1 ;
  1 2 3 4 5 6 7 8 9 10 11 12 13 14 15 16 17 18 19 20 ;
  1 2 3 4 5 6 7 8 9 10 11 12 13 14 15 16 17 18 19 20 ;
  1.50
  0.00 0.05 0.05 0.10 0.10 0.15 0.15 0.20 0.20 0.25 0.25
  0.30 0.30 0.35 0.35 0.40 0.40 0.45 0.45 0.50
  0.00 0.05 0.05 0.10 0.10 0.15 0.15 0.20 0.20 0.25 0.25
  0.30 0.30 0.35 0.35 0.40 0.40 0.45 0.45 0.50
c
  di  -1 ; 2 3 0 4 5 0 6 7 0 8 9 0 10 11 ; 1 20 ;
  di  -1 ; 12 13 0 14 15 0 16 17 0 18 19 ; 1 20 ;
  di  -1 ; 1 20 ; 2 3 0 4 5 0 6 7 0 8 9 0 10 11 ;
  di  -1 ; 1 20 ; 12 13 0 14 15 0 16 17 0 18 19 ;
c
  sii  -1 ; 1 2 0 3 4 0 5 6 0 7 8 0 9 10 0 11 12 0 13
        14 0 15 16 0 17 18 0 19 20 ;
        1 2 0 3 4 0 5 6 0 7 8 0 9 10 0 11 12 0 13
        14 0 15 16 0 17 18 0 19 20 ; 1  m
c
  coor 16 ; my -2.0 mz -2.0 ; my -1.0 mz -2.0 ; my  0.0 mz -2.0 ;
        my  1.0 mz -2.0 ; my -2.0 mz -1.0 ; my -1.0 mz -1.0 ;
        my  0.0 mz -1.0 ; my  1.0 mz -1.0 ; my -2.0 mz  0.0 ;
        my -1.0 mz  0.0 ; my  0.0 mz  0.0 ; my  1.0 mz  0.0 ;
        my -2.0 mz  1.0 ; my -1.0 mz  1.0 ; my  0.0 mz  1.0 ;
        my  1.0 mz  1.0 ;
  lrep 1 2 3 4 5 6 7 8 9 10 11 12 13 14 15 16 ;
  grep 0 1 2 3 ;
c
  velocity 0.0 0.0 0.0
c
thick 0.0400
mate 2
end
c
c

```

```
c          material model definitions
c
c tmm 1 1.31e-02
c
mat 1 3
head
  elastic-plastic model for Ti-6-4
  e 1.6e+07
  pr 0.30
  sigy 1.200e+05
  etan 3.000e+05
  beta 0.2
  ro 4.18e-04
endmat
c
mat 2 3
head
  elastic-plastic model for 2024-T3 Al
  e 1.000e+07
  pr 0.33
  sigy 5.000e+04
  etan 1.000e+05
  beta 0.2
  shell
  shear 1.0
  quad 4.0
  shth 0.040
  ro 2.53e-04
endmat
c
c
c
c bptol 3 4 0.005
c
c ptol 4 -0.01
c
c
end
c
c          interactive commands
c
c tp 0.005
c
c v
c set tv display
```

DYNA3D INPUT FILE.

This following is partial listing of the DYNA3D input file used for the fragment impact analysis. This listing contains part of each different data input section required for the analysis. However, the bulk of the input cards for various sections were eliminated to reduce the listing to a size that could be included in this appendix. The complete listing is over 100,000 lines.

```

FRAG1 - fragment penetration calculation                                88 large
*                                                                    88 large
*
*----- ANALYSIS INPUT DATA FOR DYNA3D 88 -----*
*
* Generated by Ingrid - Version # 1996e      (08/08/96)
*
*----- CONTROL CARD #2 -----*
*
* number of materials[1] nodal points[2] solid hexahedron elements[3] beam
* elements[4] 4-node shell elements[5] 8-node solid shell elements[6]
*   2      33303      3224      0      10000      0
*
*----- CONTROL CARD #3 -----*
*
* number of time history blocks for nodes[1] hexahedron elements[2] beam
* elements[3] shell elements[4] thick shell elements[5] and report interval[6]
*   0      0      0      0      0      0
*
*----- CONTROL CARD #4 -----*
*
* number of nodes in DYNA3D-JOY interface[1] number of sliding boundary
* planes[2] sliding boundary planes w/ failure[3] points in density vs depth
* curve[4] brode function flag[5] number of rigid body merge cards[6]
* nodal coordinate format[7]
*   0      0      0      0      0      0e20.0
*
*----- CONTROL CARD #5 -----*
*
* number of load curves[1] concentrated nodal loads[2] element sides having
* pressure loads applied[3] velocity/acceleration boundary condition cards[4]
* rigid walls (stonewalls)[5] nodal constraint cards[6] initial condition
* parameter[7] sliding interfaces[8] base acceleration in x[9] y[10] and
* z-direction[11] angular velocity about x[12] y[13] and z-axis[14] number of
* solid hexahedron elements for momentum deposit[15] detonation points[16]
*   0      0      0      0      0      0      1      1      0      0      0      0      0      0      0      0
*
*----- CONTROL CARD #6 -----*
*
* termination time[1] time history dump interval[2] complete dump interval[3]
* time steps between restart dumps[4] time steps between running restart
* dumps[5] initial time step[6] sliding interface penalty factor[7] thermal
* effects option[8] default viscosity flag[9] computed time step factor[10]
* 1.000E-03 1.000E-04 2.500E-05      0      0 0.000E+00 1.000E-02      0      0 7.000E-01
*
*----- CONTROL CARD #7 -----*
*
* number of joint definitions[1] rigid bodies with extra nodes[2] shell-
* solid interfaces[3] tie-breaking shell slidelines[4] tied node sets with
* failure[5] limiting time step load curve number[6] springs-dampers-masses
* flag[7] rigid bodies with inertial properties[8] dump shell strain flag[9]
* shadow burn flag[10] dump hydro variables flag[11] shell update[12]
* thickness[13] and theory options[14] number of nonreflecting
* boundary segments[15]
*   0      0      0      0      1      0      0      0      1      0      0      0      0      0      0
*
*----- CONTROL CARD #8 -----*
*
* number of point constraint nodes[1] coordinate systems for constraint
* nodes[2] minimum step factor[3] number of beam integration rules[4]
* maximum integration points for beams[5] number of shell integration rules[6]
* maximum integration points for shells[7] relaxation iterations between
* checks[8] relaxation tolerance[9] dynamic relaxation factor[10] dynamic
* relaxation time step factor[11] 4-node shell time step option[12]
*   0      0 0.000E+00      0      0      0      0      250 1.000E-04 9.950E-01 0.000E+00      0

```

```

*
*----- CONTROL CARD #9 -----*
*
* plane stress plasticity[1] printout flag[2] number of 1D slidelines[3]
  1      0      0
*
*----- MATERIAL CARDS -----*
*
  1      3 4.180E-04      0      0 0.000E+00      0 0.000E+00 0.000E+00      0      0      0
elastic-plastic model for Ti-6-4
1.600E+07 0.000E+00 0.000E+00 0.000E+00 0.000E+00 0.000E+00 0.000E+00 0.000E+00
3.000E-01 0.000E+00 0.000E+00 0.000E+00 0.000E+00 0.000E+00 0.000E+00 0.000E+00
1.200E+05 0.000E+00 0.000E+00 0.000E+00 0.000E+00 0.000E+00 0.000E+00 0.000E+00
3.000E+05 0.000E+00 0.000E+00 0.000E+00 0.000E+00 0.000E+00 0.000E+00 0.000E+00
2.000E-01 0.000E+00 0.000E+00 0.000E+00 0.000E+00 0.000E+00 0.000E+00 0.000E+00
0.000E+00 0.000E+00 0.000E+00 0.000E+00 0.000E+00 0.000E+00 0.000E+00 0.000E+00
  2      3 2.530E-04      0      0 0.000E+00      0 0.000E+00 0.000E+00      2      0      0
elastic-plastic model for 2024-T3 Al
1.000E+07 0.000E+00 0.000E+00 0.000E+00 0.000E+00 0.000E+00 0.000E+00 0.000E+00
3.300E-01 0.000E+00 0.000E+00 0.000E+00 0.000E+00 0.000E+00 0.000E+00 0.000E+00
5.000E+04 0.000E+00 0.000E+00 0.000E+00 0.000E+00 0.000E+00 0.000E+00 0.000E+00
1.000E+05 0.000E+00 0.000E+00 0.000E+00 0.000E+00 0.000E+00 0.000E+00 0.000E+00
2.000E-01 0.000E+00 0.000E+00 0.000E+00 0.000E+00 0.000E+00 0.000E+00 0.000E+00
0.000E+00 0.000E+00 0.000E+00 0.000E+00 0.000E+00 0.000E+00 0.000E+00 0.000E+00
section properties
1.000E+00 4.000E+00 3.000E+00 0.000E+00
4.000E-02 4.000E-02 4.000E-02 4.000E-02 0.000E+00
*
*----- nodal definition cards -----*
*
  1      0 0.0000000000000E+00-4.9432700000000E-01-1.4582820000000E-01      7
  2      0 0.0000000000000E+00-4.9694420000000E-01-8.3383010000000E-02      7
  3      0 0.0000000000000E+00-4.9956140000000E-01-2.0937830000000E-02      7
  4      0 0.0000000000000E+00-5.0217870000000E-01 4.1507350000000E-02      7
  5      0 0.0000000000000E+00-5.0479590000000E-01 1.0395250000000E-01      7
  6      0 0.0000000000000E+00-4.3188180000000E-01-1.4321090000000E-01      7
  7      0 0.0000000000000E+00-4.3449900000000E-01-8.0765780000000E-02      7
  8      0 0.0000000000000E+00-4.3711630000000E-01-1.8320600000000E-02      7
  9      0 0.0000000000000E+00-4.3973350000000E-01 4.4124580000000E-02      7
 10     0 0.0000000000000E+00-4.4235070000000E-01 1.0656980000000E-01      7
  .
  .
  .
33293  0 1.5000000000000E+00 1.9500000000000E+00 1.7000000000000E+00      0
33294  0 1.5000000000000E+00 1.9500000000000E+00 1.7500000000000E+00      0
33295  0 1.5000000000000E+00 1.9500000000000E+00 1.7500000000000E+00      0
33296  0 1.5000000000000E+00 1.9500000000000E+00 1.8000000000000E+00      0
33297  0 1.5000000000000E+00 1.9500000000000E+00 1.8000000000000E+00      0
33298  0 1.5000000000000E+00 1.9500000000000E+00 1.8500000000000E+00      0
33299  0 1.5000000000000E+00 1.9500000000000E+00 1.8500000000000E+00      0
33300  0 1.5000000000000E+00 1.9500000000000E+00 1.9000000000000E+00      0
33301  0 1.5000000000000E+00 1.9500000000000E+00 1.9000000000000E+00      0
33302  0 1.5000000000000E+00 1.9500000000000E+00 1.9500000000000E+00      0
33303  0 1.5000000000000E+00 1.9500000000000E+00 1.9500000000000E+00      0
*
*----- 8-node solid brick elements -----*
*
  1      1      1      26      31      6      2      27      32      7
  2      1      26      51      56      31      27      52      57      32
  3      1      51      76      81      56      52      77      82      57
  4      1      76      101     106      81      77      102     107     82
  5      1      101     126     131     106     102     127     132     107
  6      1      126     151     156     131     127     152     157     132
  7      1      151     176     181     156     152     177     182     157
  8      1      176     201     206     181     177     202     207     182

```

9	1	201	226	231	206	202	227	232	207
10	1	226	251	256	231	227	252	257	232
.									
.									
3214	1	4346	5907	5914	4353	4347	5908	5915	4354
3215	1	4353	5914	5921	4360	4354	5915	5922	4361
3216	1	3584	5532	5908	4347	3585	5533	5923	4371
3217	1	4347	5908	5915	4354	4371	5923	5926	4374
3218	1	4354	5915	5922	4361	4374	5926	5929	4377
3219	1	3585	5533	5923	4371	3586	5534	5924	4372
3220	1	4371	5923	5926	4374	4372	5924	5927	4375
3221	1	4374	5926	5929	4377	4375	5927	5930	4378
3222	1	3586	5534	5924	4372	3587	5535	5925	4373
3223	1	4372	5924	5927	4375	4373	5925	5928	4376
3224	1	4375	5927	5930	4378	4376	5928	5931	4379

*
----- 4-node shell elements -----

1	2	1292	1296	1297	1293
4.000E-02	4.000E-02	4.000E-02	4.000E-02	4.000E-02	0.000E+00
2	2	1296	1300	1301	1297
4.000E-02	4.000E-02	4.000E-02	4.000E-02	4.000E-02	0.000E+00
3	2	1300	1304	1305	1301
4.000E-02	4.000E-02	4.000E-02	4.000E-02	4.000E-02	0.000E+00
4	2	1293	1297	1298	1294
4.000E-02	4.000E-02	4.000E-02	4.000E-02	4.000E-02	0.000E+00
5	2	1297	1301	1302	1298
4.000E-02	4.000E-02	4.000E-02	4.000E-02	4.000E-02	0.000E+00
6	2	1301	1305	1306	1302
4.000E-02	4.000E-02	4.000E-02	4.000E-02	4.000E-02	0.000E+00
7	2	1294	1298	1299	1295
4.000E-02	4.000E-02	4.000E-02	4.000E-02	4.000E-02	0.000E+00
8	2	1298	1302	1303	1299
4.000E-02	4.000E-02	4.000E-02	4.000E-02	4.000E-02	0.000E+00
9	2	1302	1306	1307	1303
4.000E-02	4.000E-02	4.000E-02	4.000E-02	4.000E-02	0.000E+00
10	2	1295	1299	1343	1336
4.000E-02	4.000E-02	4.000E-02	4.000E-02	4.000E-02	0.000E+00
.					
.					
.					
9991	2	33285	7814	7815	33286
4.000E-02	4.000E-02	4.000E-02	4.000E-02	4.000E-02	0.000E+00
9992	2	33287	7815	7816	33288
4.000E-02	4.000E-02	4.000E-02	4.000E-02	4.000E-02	0.000E+00
9993	2	33289	7816	7817	33290
4.000E-02	4.000E-02	4.000E-02	4.000E-02	4.000E-02	0.000E+00
9994	2	33291	7817	7818	33292
4.000E-02	4.000E-02	4.000E-02	4.000E-02	4.000E-02	0.000E+00
9995	2	33293	7818	7819	33294
4.000E-02	4.000E-02	4.000E-02	4.000E-02	4.000E-02	0.000E+00
9996	2	33295	7819	7820	33296
4.000E-02	4.000E-02	4.000E-02	4.000E-02	4.000E-02	0.000E+00
9997	2	33297	7820	7821	33298
4.000E-02	4.000E-02	4.000E-02	4.000E-02	4.000E-02	0.000E+00
9998	2	33299	7821	7822	33300
4.000E-02	4.000E-02	4.000E-02	4.000E-02	4.000E-02	0.000E+00
9999	2	33301	7822	7823	33302
4.000E-02	4.000E-02	4.000E-02	4.000E-02	4.000E-02	0.000E+00
10000	2	33303	7823	7696	7689
4.000E-02	4.000E-02	4.000E-02	4.000E-02	4.000E-02	0.000E+00

*

---- initial conditions (velocities) ----

*

1	2.323E+03	0.000E+00	0.000E+00	0
2	2.323E+03	0.000E+00	0.000E+00	0
3	2.323E+03	0.000E+00	0.000E+00	0
4	2.323E+03	0.000E+00	0.000E+00	0
5	2.323E+03	0.000E+00	0.000E+00	0
6	2.323E+03	0.000E+00	0.000E+00	0
7	2.323E+03	0.000E+00	0.000E+00	0
8	2.323E+03	0.000E+00	0.000E+00	0
9	2.323E+03	0.000E+00	0.000E+00	0
10	2.323E+03	0.000E+00	0.000E+00	0
.				
.				
.				
33293	0.000E+00	0.000E+00	0.000E+00	0
33294	0.000E+00	0.000E+00	0.000E+00	0
33295	0.000E+00	0.000E+00	0.000E+00	0
33296	0.000E+00	0.000E+00	0.000E+00	0
33297	0.000E+00	0.000E+00	0.000E+00	0
33298	0.000E+00	0.000E+00	0.000E+00	0
33299	0.000E+00	0.000E+00	0.000E+00	0
33300	0.000E+00	0.000E+00	0.000E+00	0
33301	0.000E+00	0.000E+00	0.000E+00	0
33302	0.000E+00	0.000E+00	0.000E+00	0
33303	0.000E+00	0.000E+00	0.000E+00	0

*

---- sliding interface control cards ----

*

624	6400	3	0.000E+00	0.000E+00	0.000E+00	0	0	00.0E+000.0E+00
1	351	352	357	356				
2	352	353	358	357				
3	353	354	359	358				
4	354	355	360	359				
5	356	357	362	361				
6	357	358	363	362				
7	358	359	364	363				
8	359	360	365	364				
9	361	362	367	366				
10	362	363	368	367				
.								
.								
.								
613	350	900	940	375				
614	900	905	945	940				
615	905	910	950	945				
616	910	915	955	950				
617	915	920	960	955				
618	920	925	965	960				
619	925	930	970	965				
620	930	935	975	970				
621	935	1240	1260	975				
622	1240	1245	1265	1260				
623	1245	1250	1270	1265				
624	1250	1255	1275	1270				
1	5980	6461	8340	6589				
2	6461	6462	8342	8341				
3	6462	6463	8344	8343				
4	6463	6464	8346	8345				
5	6464	6465	8348	8347				
6	6465	6466	8350	8349				
7	6466	6467	8352	8351				
8	6467	6468	8354	8353				
9	6468	6469	8356	8355				
10	6469	6470	8358	8357				

```

.
.
.
6390 33283 7682 7689 33284
6391 33285 33286 7815 7814
6392 33287 33288 7816 7815
6393 33289 33290 7817 7816
6394 33291 33292 7818 7817
6395 33293 33294 7819 7818
6396 33295 33296 7820 7819
6397 33297 33298 7821 7820
6398 33299 33300 7822 7821
6399 33301 33302 7823 7822
6400 33303 7689 7696 7823

```

```

*
*----- tied nodes with failure -----*
*

```

```

6241 4
2.000E-01
2.000E-01 8340 8341 8359 8361
2.000E-01 8342 8343 8362 8365
2.000E-01 8344 8345 8366 8369
2.000E-01 8346 8347 8370 8373
2.000E-01 8348 8349 8374 8377
2.000E-01 8350 8351 8378 8381
2.000E-01 8352 8353 8382 8385
2.000E-01 8354 8355 8386 8389
2.000E-01 8356 8357 8390 8393

```

```

.
.
2.000E-01 33236 33239 33272 33275
2.000E-01 33240 33243 33276 33279
2.000E-01 33244 33246 33280 33283
2.000E-01 33250 33253 33286 33287
2.000E-01 33254 33257 33288 33289
2.000E-01 33258 33261 33290 33291
2.000E-01 33262 33265 33292 33293
2.000E-01 33266 33269 33294 33295
2.000E-01 33270 33273 33296 33297
2.000E-01 33274 33277 33298 33299
2.000E-01 33278 33281 33300 33301
2.000E-01 33282 33284 33302 33303

```